

2
(NASA-CR-138521) INTERIOR RADIANCES IN
OPTICALLY DEEP ABSORBING MEDIA. 3:
SCATTERING FROM HAZE L (Texas A&M Univ.)
57 p HC \$6.00 CSCL 20F

N74-27191

G3/23 41173
Unclas

Interior Radiances in Optically Deep Absorbing Media--III

Scattering from Haze L

by

George W. Kattawar and Gilbert N. Plass

Report No. 9

The research described in this report was

funded by the

National Aeronautics and Space Administration

Contract No. NGR 44-001-117

Department of Physics
Texas A & M University
College Station, Texas 77843



June 13, 1974

A paper based on the material in this report has been submitted to the Journal of Quantitative Spectroscopy and Radiative Transfer.

Interior Radiances in Optically Deep Absorbing Media -- III

Scattering from Haze L

George W. Kattawar and Gilbert N. Plass

Department of Physics, Texas A&M University, College Station, Texas 77843, U.S.A.

Abstract

The interior radiances are calculated within an optically deep absorbing medium scattering according to the Haze L phase function. The dependence on the solar zenith angle, the single scattering albedo, and the optical depth within the medium is calculated by the matrix operator method. The development of the asymptotic angular distribution of the radiance in the diffusion region is illustrated through a number of examples; it depends only on the single scattering albedo and on the phase function for single scattering. The exact values of the radiance in the diffusion region are compared with values calculated from the approximate equations proposed by Van de Hulst. The variation of the radiance near the lower boundary of an optically thick medium is illustrated with examples. The attenuation length is calculated for various single scattering albedos and compared with the corresponding values for Rayleigh scattering. The ratio of the upward to the downward flux is found to be remarkably constant within the medium. The heating rate is calculated and found to have a maximum value at an optical depth of two within a Haze L layer when the sun is at the zenith. The location of this maximum moves toward the top of the haze layer as the solar zenith angle increases and also as the single scattering albedo decreases. When the single scattering albedo is less than 0.8, the downward flux is so small within the diffusion region that experimental measurements are probably not possible.

INTRODUCTION

The interior radiance within optically deep absorbing media may be calculated by the matrix operator theory recently reviewed by Plass et al. ⁽¹⁾. An entirely rigorous numerical solution of the radiative transfer equations is obtained by this method. Further details of the matrix operator method are given in the first part of this series of articles by Kattawar and Plass ⁽²⁾ (hereafter referred to as I). In the second part by Plass et al. ⁽³⁾ (hereafter referred to as II), results are given for the interior radiance within a medium with Rayleigh scattering.

The only reasonably accurate values for the interior radiance previously reported in the literature appear to be those of Plass and Kattawar ^(4,5) and Kattawar and Plass. ⁽⁶⁾ Interior radiances were calculated by a Monte Carlo technique for the earth's atmosphere-ocean system taking into account the optical properties of the interface between the atmosphere and ocean.

The present results obtained by the matrix operator technique essentially use the relatively simple equation for the interior radiance originally given by Bellman ⁽⁷⁾ (see equations (3-4) on p. 348) which do not appear to have been used previously in practical calculations.

The only difference between the calculations reported here and those for Rayleigh scattering given in II is the use of a Haze L phase function as defined by Deirmendjian ⁽⁸⁾ for the present calculations. The size distribution of the radii of the haze particles is proportional to $r^6 \exp(-15.1186 r^{\frac{1}{2}})$. The modal radius is 0.63 μ . A method for the calculation of the Mie phase matrix in an efficient form for use in matrix operator calculations is given by Kattawar et al. ⁽⁹⁾

The results of the present calculations illustrate the dependence of the interior radiance and flux on the optical depth within the medium as well as on its absorbing and scattering properties. The development of the asymptotic angular distribution of the radiance in the diffusion region is given. This

asymptotic distribution is unobservable when the single scattering albedo is small, since the diffusion region only begins at great optical depths where the flux is extremely small. The range of optical depths where the ratio of the upward to downward flux is constant is investigated, as is the range where the decrease of the downward flux with optical depth can be represented by an exponential. The heating rate within the medium is calculated and found to be nearly proportional to the downward flux except near the boundaries. The results for the Haze L scattering function are compared with those for Rayleigh scattering.

DOWNWARD RADIANCE

The phase function calculated from Mie theory for the distribution of particle sizes known as Haze L is shown in Fig. 1. The real part of the index of refraction was taken as 1.55 in all cases. The phase function was calculated for five different values of the complex part of the refractive index: $n_2 = 0.0; 0.001; 0.0127; 0.028; 0.23$. The single scattering albedo ω_0 is defined as the fraction of the incident light lost by scattering whereas a fraction $1 - \omega_0$ is lost by absorption in a single event. The corresponding values of ω_0 for the five different values of n_2 given above are: 1.000; 0.989; 0.890; 0.801; 0.503. The average value of the cosine of the scattering angle (g) for each of these cases is respectively: 0.6583; 0.6682; 0.6911; 0.7206; 0.8326. For clarity these phase functions have been displaced vertically in Fig. 1. The value of unity on each phase function has been marked by a short horizontal line.

The dashed lines in Fig. 1 show the analytic phase function which has been used extensively in the literature and which was introduced by Henyey and Greenstein⁽¹⁰⁾. This phase function is defined as

$$\phi(\mu) = (4 \pi)^{-1} (1-g^2) (1+g^2 - 2g\mu)^{-3/2}, \quad (1)$$

whose normalization is

$$\int_{-1}^1 \int_0^{2\pi} \phi(\mu) d\mu d\phi = 1. \quad (2)$$

The values of g calculated from the exact Mie phase function as given above were used to plot the Henyey-Greenstein phase function. The approximate phase function does not reproduce the actual increase in the Mie phase function for scattering angles near 180° (the glory) for the first four phase functions nor does it reproduce the sharpness of the forward scattering peak for scattering angles near 0° . Only when the absorption is quite large ($n_2 = 0.23$, $\omega_0 = 0.503$) does it approximate the Mie phase function. The accurate phase function obtained from Mie theory has been used in all of the matrix operator calculations given here. They are included in the calculation by the method described by Kattawar et al. ⁽⁹⁾

The interior radiances were calculated from equations (5) and (6) of Plass et al. ⁽¹⁾ by the methods of matrix operator theory. Greatly improved accuracy was obtained by the use of a Runge-Kutta method to obtain a starting value instead of using the single scattering approximation. The differential equations satisfied by the reflection and transmission operators (see Kattawar ⁽¹¹⁾) were integrated from the origin to an optical depth of the order of 10^{-3} . Since the error of the Runge-Kutta method is proportional to h^5 where h is the interval size, the solution at this optical depth has an error of the order of 10^{-15} . These calculations were done on a CDC 7600 and required approximately 8 min of computer time for each of the five cases reported here.

The calculations were continued out to very large ($\tau = 16,794$) optical depths when the single scattering albedo $\omega_0 = 1$; when $\omega_0 < 1$ the calculations were carried out to optical depths of 65-109 depending on the particular value

of ω_0 . In each case results were calculated using several different values for the albedo of the lower surface. Since this albedo only influences the radiance near the lower surface, it is only of interest when studying the radiance near this surface.

The downward normalized diffuse radiance is shown in Fig. 2 when $\omega_0 = 1$ as a function of the cosine μ of the zenith angle of observation. These curves are in the principal plane, so the azimuthal angle $\phi = 0^\circ$ or 180° . The cosine μ_0 of the solar zenith angle is 0.85332 which corresponds to a zenith angle $\theta_0 = 31.42^\circ$. The downward radiance is shown for a number of different values of the optical depth τ within the medium. In each case the radiance is multiplied by the factor $(\pi/\text{diffuse flux at depth } \tau)$, so that the variation of the radiance with μ at different depths can conveniently be compared. The incoming flux is normalized to unity across a plane perpendicular to the incoming beam.

At small values of the optical depth there is a pronounced maximum in the downward radiance due to the strong forward scattering of the Haze L phase function. At $\tau = 5$ this maximum has become weak and is nearer the zenith. The asymptotic radiance distribution exists for $\tau > 13$ on the scale of this figure. The development of an asymptotic form for the radiance distribution at large optical depths was predicted by Preisendorfer⁽¹²⁾, but no calculations have previously been reported of its development with optical depth, other than those in II.

The downward normalized interior radiance for $\omega_0 = 0.99, 0.9, 0.8$ and 0.5 is shown in Figs. 3-6 respectively. When $\tau < 1$ the angular dependence of the radiance remains qualitatively the same as ω_0 decreases, the only effect being a slight increase in the value at the maximum and a corresponding decrease at the minima. On the other hand the angular dependence for large values of

τ depends critically on ω_0 . The ratio of the radiance at the zenith to that at the horizon increases greatly as ω_0 becomes smaller. The optical depth required for the development of the asymptotic form on the scale of these figures increases as ω_0 increases; the asymptotic form is approximately valid for $\tau > 17$ when $\omega_0 > 0.8$, but only when $\tau > 33$ when $\omega_0 = 0.5$.

Preisendorfer⁽¹²⁾ was only able to derive the variation of the radiance with μ at large optical depths in the diffusion region for the special case of isotropic scattering. In II the results for Rayleigh scattering are given, which agree approximately with the predictions for isotropic scattering. No other results have been reported previously for other scattering functions. Thus it is of considerable interest to study the variation of the asymptotic radiance distribution as the phase function is changed.

In the diffusion region the ratio of the upward radiance at the nadir ($\mu = 1$) to that at the closest calculated point to the horizon ($\mu = 0.03785$) is shown in columns 2 and 3 of Table 1 for both the Rayleigh and Haze L phase functions. The ratio of the downward diffuse radiance at the zenith ($\mu = 1$) to that at the closest calculated point to the horizon ($\mu = 0.03785$) is shown in columns 4 and 5. In the diffusion region the radiance at any particular value of μ decreases as $\exp(-b\tau)$; the value of the attenuation length b is given in columns 6 and 7 of this table.

The value of b is less for Haze L than for Rayleigh phase functions for all values of ω_0 . The stronger forward scattering in the former case allows the photons to reach greater optical depths. Thus the downward flux is greater for Haze L than for Rayleigh scattering at any particular optical depth such that $\tau > 1$. A consequence is that the value of b must be less than for Rayleigh scattering.

The ratio of the downward flux at the zenith to that near the horizon as given in Table 1 shows that this ratio is larger for Haze L than for Rayleigh scattering for all values of ω_0 , because of the greatly

increased forward scattering in the former case. When $\omega_0 \leq 0.8$, the downward radiance is largely concentrated in a relatively narrow solid angle around the zenith.

The dependence of the ratio of the upward radiance at the nadir to that near the horizon as given in Table 1 is more complicated. For Rayleigh scattering, the ratio first decreases and then increases as ω_0 decreases. On the other hand, the ratio monotonically decreases over the calculated range as ω_0 decreases for Haze L scattering. The upward radiance is derived by multiple scattering from the downward. The described variation of the ratio can be understood by consideration of an approximation valid for small values of ω_0 . When $\omega_0 \leq 0.5$ most of the photons in the upward beam in the diffusion region have undergone only a single scattering after leaving the downward beam, because of the high probability of absorption for these values of ω_0 . Furthermore the downward beam can be considered to be approximately in the vertical direction in the diffusion region. In this approximation an elementary integration over τ of the probability for single scattering shows that

$$I^{\text{up}}(1)/I^{\text{up}}(\mu) = [\phi(-1)/\phi(-\mu)][\frac{1}{2}(1+\mu)], \quad (3)$$

where ϕ is any single scattering phase function. When $\mu = 0.03785$ the approximate ratio predicted from this equation is 1.036 for Rayleigh scattering and 0.24 for Haze L scattering. The ratio for Rayleigh scattering is approaching

this approximate value when $\omega_0 = 0.1$. Calculations were not made for Haze L scattering for this value of ω_0 , but the ratio probably increases from its value of 0.162 when $\omega_0 = 0.5$ to more nearly agree with the approximate formula. In any case the approximate equation indicates how the upward radiance depends on the phase function.

The variation of the flux and radiance as a function of optical depth is given in Tables 2 - 6 for $\omega_0 = 1, 0.99, 0.9, 0.8, 0.5$ and for the sun at the zenith. The optical depth is given in the first column. In each case the lower boundary of the medium was taken at the largest optical depth shown in each table. A lower boundary surface with zero albedo was assumed. The values for the flux and heating rates are discussed in later sections. In all cases the incident solar flux is normalized to a value of unity through a surface perpendicular to its initial direction.

The last two columns of Table 2 - 6 show the ratio of the upward radiance at the nadir to that near the horizon ($\mu = 0.03785$ or $\theta = 87.83^\circ$) and the ratio of the downward diffuse radiance at the zenith to that near the horizon. When $\omega_0 = 1$, these ratios become very close to unity in the interior of a medium of total optical thickness 16,794. When $\omega_0 = 0.5$, this ratio for the downward radiance can become large (139 at $\tau = 2.98$). These ratios can be used as a test for the optical depth at which the asymptotic radiance distribution begins, since these ratios do not change within the diffusion region. When $\omega_0 = 0.99$ these ratios are constant to five significant figures if $25 < \tau < 53$. When $\omega_0 = 0.8$ these ratios are constant to three significant figures if $25 < \tau < 65$. However, in this case, the downward flux is 2.8×10^{-5} at $\tau = 25$ and 7.5×10^{-13}

at $\tau = 65$. Thus experimental measurements could only be made with difficulty, if at all, due to the low light levels and interference from other light sources in this diffusion region. When $\omega_0 = 0.5$, these ratios are constant within one percent only when $33 < \tau < 61$. The downward flux is only 3.9×10^{-10} at $\tau = 33$. Thus, when $\omega_0 < 0.8$, the radiance is too small for experimental measurement within the diffusion region. A similar conclusion was reached in II for Rayleigh scattering.

The downward interior radiance when the sun is near the horizon, $\omega_0 = 0.18816$ ($\theta_0 = 79.15^\circ$), is shown in Figs. 7 and 8 for $\omega_0 = 0.99$ and 0.5 respectively. It is interesting to follow the position of the maximum value of the downward radiance as the optical depth of observation within the medium increases. For very small optical depths the maximum downward radiance is at the horizon. At a depth $\tau = 0.5$ within the medium the maximum is near 79° (close to the solar direction). When $\tau = 1$, the maximum has moved to about 75° . When $\tau = 3$, the maximum is near 49° and 53° for $\omega_0 = 0.99$ and 0.5 respectively. It is near 32° and 36° at $\tau = 5$ and near 5° and 14° at $\tau = 9$; in each case the values are for $\omega_0 = 0.99$ and 0.5 respectively. When $\omega_0 = 0.99$ the maximum value is at the zenith for all $\tau > 13$. This is true for $\omega_0 = 0.5$, when $\tau > 21$.

All of the radiance values presented so far have been in the principal plane which contains the incident solar direction. Some examples of the azimuthal variation of the downward radiance are given in Figs. 9 and 10. As before the actual downward radiance has been multiplied in each case by the factor $(\pi/\text{diffuse downward flux at depth } \tau)$, so that the variation of the radiance with μ at different depths can conveniently be compared.

The downward normalized radiance is shown in the lower part of Fig. 9 when $\mu_0 = 0.18817$ ($\theta_0 = 79.15^\circ$), $\mu = 0.26192$ ($\theta = 74.82^\circ$) and $\omega_0 = 1$. At small optical depths the radiance is maximum in the solar direction ($\phi = 0^\circ$) and a minimum in the antisolar direction ($\phi = 180^\circ$). At optical depths greater than 13 the radiance is independent of the azimuthal angle on the scale of this figure.

As another example the downward radiance is shown in Fig. 10 for $\mu_0 = 0.85332$ ($\theta_0 = 31.42^\circ$), $\mu = 0.71392$ ($\theta = 44.44^\circ$) and $\omega_0 = 0.5$. When there is appreciable absorption within the medium, as in this case, the variation with azimuthal angle persists to much greater optical depth than otherwise. In this case it is only at optical depths greater than 33 that the downward radiance is independent of ϕ on the scale of this figure. This is another indication that the diffusion region has been reached.

UPWARD RADIANCE

The upward normalized radiance is shown in Figs. 11 - 14 for $\omega_0 = 1.0$, 0.99, 0.8, and 0.5. As in the case of the downward radiance, the upward normalized radiance is computed by multiplying the upward radiance by the factor ($\pi/\text{diffuse upward flux at depth } \tau$). The radiance in these figures is shown as a function of the cosine μ of the nadir angle and is for the incident plane ($\phi = 0^\circ$ or 180°). The cosine of the solar zenith angle was chosen as $\mu_0 = 0.85332$ (31.42°). As expected the variation of the upward radiance with μ is very much less than that for the downward radiance.

When $\omega_0 = 1$ (see Fig. 11) the upward radiance above a thick haze layer increases from the solar horizon (left side of all figures for upward radiance) to the nadir and then continues to increase to a relatively sharp maximum at $\mu = 0.835$; the radiance then decreases to the antisolar horizon (right side of figures). The

maximum is due to the glory phenomenon, the increase in the phase function for scattering angles from about 120° to 180° (see Fig. 1). The relatively rapid increase in the phase function as the scattering angle approaches 180° is the reason for the maximum in these radiance curves. No maximum whatsoever would have been obtained if the Henyey-Greenstein phase function had been used since it has no maximum for backward scattering. This maximum still occurs at an optical depth of unity for a haze with $\omega_0 = 1$, but cannot be seen on the scale of the figure when $\tau = 5$.

The upward radiance at the top of the haze layer ($\tau = 0$) is somewhat different when $\omega_0 = 0.99$ (Fig. 12). The radiance increases from the solar horizon to a maximum near $\mu = 70^\circ$ and then decreases until near the nadir; the radiance then increases to a stronger maximum near $\mu = 0.853$ than in the previous case with $\omega_0 = 1$; the radiance then decreases to the antisolar horizon. The maximum is stronger than in the previous case because of the small amount of absorption which decreases the contribution from multiple scattering. A trace of the relative maximum for 180° single scattering can still be seen at an optical depth of 3 within the medium. The asymptotic form for the upward radiance is reached in this case on the scale of the figure at $\tau = 9$; the radiance increases from the nadir toward the horizon.

When $\omega_0 = 0.8$ (Fig. 13) the maximum near the angle for 180° single scattering is somewhat less than in the two previous figures, but is still noticeable for $\tau < 3$. The phase function still has a maximum at 180° in this case (Fig. 1). The radiance at the solar horizon is larger than that at the nadir at all optical depths.

The variation of the upward radiance with μ is quite different when $\omega_0 = 0.5$ (Fig. 14). There is no longer any maximum near $\mu = 0.853$. The phase function (Fig. 1) does not have a relative maximum for 180° scattering when the particles absorb this much. At all optical depths from the top of the haze layer to within

the diffusion region, the upward radiance has qualitatively the same variation with μ in this case.

The upward radiance when the sun is near the horizon ($\mu_0 = 0.18816$; $\theta_0 = 79.15^\circ$) is shown in Fig. 15 for the case $\omega_0 = 0.5$. There is a much larger variation in the upward radiance (three orders of magnitude near the top of the haze layer) than in the previous cases considered. The asymptotic radiance distribution does not develop (on the scale of Figs. 14 and 15) until optical depths of the order of 33 are reached.

Two examples of the variation of the upward radiance with azimuthal angle ϕ are given in Figs. 9 and 16 for $\mu_0 = 0.18816$ and $\mu = 0.26192$. When $\omega_0 = 1$ (Fig. 9), the radiance is a minimum near $\phi = 120^\circ$ at small optical depths. On the other hand when $\omega_0 = 0.5$ (Fig. 16), the radiance decreases monotonically with ϕ . There is a larger variation with ϕ in the latter case and the radiance does not become independent of ϕ on the scale of the figure until $\tau = 33$.

APPROXIMATE RADIANCE EQUATION

Van de Hulst¹³ obtained the following approximate expressions for the radiance $R(\mu)$ in the diffusion region and the approximate single scattering albedo ω_A ,

$$R(\mu) = 1 + (1-g)^{-1} b\mu + \frac{2}{3} (1-g)^{-1} (1-h)^{-1} b^2 P_2(\mu) + \dots, \quad (4)$$

$$\omega_A = 1 - \frac{1}{3} (1-g)^{-1} b^2 - [(4-9g + 5gh)/45(1-g)^3(1-h)]b^4 + \dots, \quad (5)$$

where in our convention

$$g = \int_0^{2\pi} \int_{-1}^1 \Phi(\mu) P_1(\mu) d\mu d\phi, \quad (6)$$

$$h = \int_0^{2\pi} \int_{-1}^1 \Phi(\mu) P_2(\mu) d\mu d\phi, \quad (7)$$

where $\Phi(\mu)$ is any single scattering phase function normalized according to equation (2), $P_1(\mu)$ and $P_2(\mu)$ are Legendre polynomials (μ and $\frac{1}{2}(3\mu^2 - 1)$ respectively), b is the attenuation length in the asymptotic radiance region as tabulated in Table 1. The single scattering albedo and the radiance were calculated for each haze phase function from these approximate equations.

These approximate results were checked against our exact calculations. The value of the attenuation length was taken from the exact matrix operator calculations. The approximate equations for the radiance are accurate for all values of μ within 0.55% when $\omega_0 \geq 0.99$. These approximate equations, however develop inaccuracies rapidly as ω_0 departs further from unity. When the exact value of the single scattering albedo $\omega_E = 0.900$, the approximate single scattering albedo calculated from equation (2), $\omega_A = 0.901$; the calculated downward and upward radiance from equation (4) is given in Fig. 17. The downward and upward radiances calculated from equation (4) have errors as large as 5.7% and 29.6% at the zenith when $\omega_0 = 0.9$.

Similarly when $\omega_E = 0.800$, the value obtained from equation (5) is $\omega_A = 0.813$; the radiances are shown in Fig. 18. The approximate equation is considerably less accurate for the upward than for the downward radiance with large discrepancies obvious in these two cases. When $\omega_E = 0.800$, the upward radiance calculated from equation (4) is in error by 204% near $\mu = 1$ and by 149% near $\mu = 0.54$; the downward radiance also calculated from equation (4) is in error by 14% near $\mu = 1$ and 29% near $\mu = 0.54$. Thus the approximate expressions developed by Van de Hulst given by equations (4) and (5) are reasonably accurate only when $\omega_0 \geq 0.99$.

In the diffusion region both the total downward flux as well as the radiance at a particular angle decreases as $\exp(-b\tau)$. The accurate values of b obtained from the matrix operator calculations as a function of ω_0 are shown in the center part of Fig. 19 for both Rayleigh and Haze L phase

functions.

Van de Hulst¹³ gives the following approximate expression for b

$$b^2 = 3(1 - \omega_0)(1 - g) + \dots \quad (8)$$

The ratio $b^2/3(1 - \omega_0)(1 - g)$ should be constant if b is given by the first term of this expansion. This ratio is shown in the lower part of Fig. 19. Obviously this is a poor expression for b unless ω_0 is near unity.

RADIANCE NEAR LOWER BOUNDARY

A Lambert reflecting surface is assumed in these calculations at the lower boundary of the optically thick medium. Neither this assumption nor the albedo of the lower surface, A , has any influence on the radiance in the diffusion region far in the interior of the medium. On the other hand the variation of the radiance with optical thickness from the boundary is entirely different at the lower boundary than at the upper because of the entirely different boundary conditions. Near the upper boundary the radiance is strongly dependent on the solar zenith angle and is in general also a function of the azimuthal angle. In the diffusion region deep inside the medium, the photons have made so many collisions that they have lost all memory of the initial solar direction. The radiance no longer depends on the solar zenith angle and is independent of the azimuthal angle of observation. The radiance from the lower boundary up into the diffusion region of an optically deep medium does not depend on the solar zenith angle nor on the azimuthal angle of observation for the same reason just mentioned.

Thus the development of the radiance from the lower boundary into the medium is entirely different than that from the upper. Some examples are given here. Both the upward and downward normalized radiance are given in Fig. 20 when $\omega_0 = 1$ and $A = 0$. The total optical depth of the medium was 16,794, so that the radiance in the region shown here is independent of both μ_0 and ϕ . 15<

The optical depth measured from the lower boundary is called τ' . At the lower boundary the downward radiance increases monotonically from the horizon to the zenith. The variation with μ becomes progressively less pronounced as τ' increases. At $\tau' = 77$ the downward radiance is equal to its asymptotic form on the scale of the figure. Because of the assumption that $A = 0$, the upward radiance is zero at the lower boundary. The upward normalized radiance when $\tau' = 0.125$ is shown in the upper part of Fig. 20; it decreases monotonically from the horizon to the nadir. The upward radiance has approached its asymptotic form when $\tau' = 77$.

As another example, the downward and upward normalized radiance when $\omega_0 = 0.8$ and $A = 0$ and 0.15 is shown in Figs. 21 and 22. In this case there is relatively little change in the downward normalized radiance from the lower boundary into the asymptotic region. At $\tau' = 3$ it is equal to the asymptotic form on the scale of this figure. There is also relatively little difference between the curves for $A = 0$ and $A = 0.15$ except near the horizon.

As might be expected the upward normalized radiance is much more sensitive to the value of the surface albedo as shown in Fig. 22. It approaches the asymptotic form when $\tau' = 9$ on the scale of this figure. When $A = 0$ the upward normalized radiance decreases by over two orders of magnitude from the horizon to the nadir when $\tau' = 0.009766$. As τ' increases the value near the horizon decreases and the value near the nadir increases to the correct asymptotic value. The variation is just the opposite when $A = 0.15$. The upward normalized radiance is constant at $\tau' = 0$ because of the assumed Lambert bounding surface. As τ' increases, the value near the horizon increases and the value near the nadir decreases until the asymptotic value is reached. The limiting asymptotic curve for the radiance is, of course, independent of the assumed value for the surface albedo, A .

FLUX

Flux values at various optical depths within the medium are given in Table 2 when $\omega_0 = 1$, and $\mu_0 = 1$. The second column gives the upward flux; the third column shows the downward diffuse flux; the fourth column gives the total downward flux including the incident solar beam, which is assumed to be at the zenith. The difference between the total downward flux and the upward flux is shown in the fifth column. The upward and downward flux have the same numerical value to four or five significant figures down to optical depths of several thousand. Nevertheless their difference is constant to three significant figures in our calculations. This difference is necessarily a constant for a conservative problem ($\omega_0 = 1$). The incident solar beam makes no contribution to the total downward flux to five significant figures at optical depths greater than 13. The total downward flux becomes significantly greater than unity over a large range of optical depths starting from the upper surface as is the case for Rayleigh scattering (see II). When $\tau > 5$, the total downward flux is always greater for the Haze L than for the Rayleigh scattering medium. This is due to the greater forward scattering from the haze phase function and persists down to an optical depth of 16,794 at the lower surface of the medium, even though the photons which reach this level have undergone an extremely large number of scattering events.

The first four columns in Tables 3-6 tabulate the same quantities as are in the corresponding columns of Table 2. The fifth column of Tables 3-6 shows the ratio of the upward flux to the total downward flux. The quantity $\partial F / \partial \tau$, which is proportional to the heating rate of the layer, is given in the sixth column.

Within the tabulated accuracy of four significant figures, the incident beam does not contribute to the total flux at optical depths greater than 17 when $\omega_0 = 0.99$, 0.9, or 0.8. When $\omega_0 = 0.5$, the incident beam does not contribute at optical depths greater than 33. This is quite different for Rayleigh scattering (see II) where the incident beam makes a significant contribution at much larger optical depths. The stronger forward scattering from Haze L than from Rayleigh is the reason for much higher flux values at corresponding levels deep within a Haze L compared to a Rayleigh medium. For example, at $\tau = 40.98$ the ratio of the downward diffuse flux for Haze L to that for Rayleigh is 19, 5,768, and 55,420 for $\omega_0 = 0.99$, 0.9, and 0.5 respectively. An important consequence of this is that the direct solar beam makes a significant contribution to the flux and radiance at deeper levels for Rayleigh than for Haze L scattering, especially when there is appreciable absorption in the medium. This in turn is an important factor in determining the optical depth at which the diffusion region first develops. The diffusion region cannot develop as long as the direct solar beam is a significant fraction of the radiance in that direction.

A quantity which is often measured experimentally is the ratio of the upward interior flux to the total downward interior flux. This ratio is remarkably constant over a large range of optical thickness in an optically deep medium. The limiting value of this ratio in the diffusion region is determined only by the phase function and the single scattering albedo. Since the upward flux is derived by multiple scattering from the downward flux, this ratio only changes near boundaries where other factors have an influence.

When $\omega_0 = 0.99$, the ratio of the upward to downward interior flux is 0.673 and is constant from $9 \leq \tau \leq 69$ for a medium of total optical depth of 109. The corresponding value of the ratio for Rayleigh scattering is 0.793. The ratio is always larger for Rayleigh scattering than for Haze L because of the larger probability for backward scattering in the first case. When $\omega_0 = 0.9$, the ratio is 0.265 (compared to 0.470 for Rayleigh) when $17 \leq \tau \leq 65$ for a medium of total optical depth of 77. When $\omega_0 = 0.8$, the ratio is 0.136 when $17 \leq \tau \leq 65$ for a medium of total optical depth of 77. Finally when $\omega_0 = 0.5$, the ratio is 0.0171 (compared to 0.132 for Rayleigh) when $25 \leq \tau \leq 61$ for a medium of total optical depth of 65. Since the diffusion region only begins at approximately $\tau = 25$ when $\omega_0 = 0.5$, it would be extremely difficult to observe the flux or radiance in this region since the total downward flux is only 8.756×10^{-8} at $\tau = 25$. The ratio is not only much lower for Haze L than for Rayleigh when $\omega_0 = 0.5$, but the diffusion region is established at a much smaller optical depth in the former case.

The heating rate is proportional to the quantity $\partial F/\partial \tau$, which is also given in Tables 3-6. In the diffusion region the heating rate is proportional to the downward flux. The ratio of $\partial F/\partial \tau$ to the total downward flux in this region is 0.03311, 0.2293, 0.3771, and 0.6642 when $\omega_0 = 0.99, 0.9, 0.8,$ and 0.5 respectively. The corresponding values for Rayleigh scattering are 0.03564, 0.2775, and 0.818 for $\omega_0 = 0.99, 0.9,$ and 0.5 respectively. The variation of this ratio with ω_0 is shown in Fig. 19.

The heating rate as a function of optical depth within the medium is shown in Fig. 23 when $\omega_0 = 0.99$ for various values of μ_0 . All of these curves have been normalized to the value unity at $\tau = 0$. When the sun is at the zenith the maximum heating occurs at an optical depth $\tau = 2$ within the haze layer. When $\mu_0 = 0.85332$ (31.43°), the maximum heating occurs at approximately $\tau = 1.4$. As the

sun moves away from the zenith the region of maximum heating rapidly approaches the top of the haze layer. It is at approximately $\tau = 0.2$ when $\mu_0 = 0.53786$ (57.46°). This fact may have important consequences on the development of clouds.

The heating rate as a function of optical depth within the medium is shown in Fig. 24 when $\mu_0 = 1$ and 0.18816 (79.15°) for various values of ω_0 . When $\mu_0 = 1$, the optical depth at which the maximum heating rate occurs moves towards the top of the haze layer as ω_0 decreases; it is approximately at $\tau = 2, 0.7,$ and 0.2 when $\omega_0 = 0.99, 0.9,$ and 0.8 respectively. When the sun is near the horizon, the heating rates decrease very much more rapidly as τ increases than when it is at the zenith.

CONCLUSIONS

The variation of the flux and radiance within a very thick Haze L scattering-absorbing layer has been studied and illustrated through a number of examples. The dependence on the solar zenith angle, the single scattering albedo, and the optical depth within the medium is shown. These results are compared with those for Rayleigh scattering.

A diffusion region always exists in the interior of a sufficiently thick medium. Within this region the upward and downward radiance is independent of the solar zenith angle, of the azimuthal angle of observation, and of the albedo of the lower surface. The asymptotic radiance distribution in this region depends only on the single scattering albedo and on the phase function for single scattering. A necessary condition for the existence of the diffusion region at a given depth within the medium is that the direct solar beam be very small compared to the radiance in the same direction. The ratio of the downward (upward) radiance at

the zenith (nadir) to that near the horizon approaches a limiting value as the optical depth increases and the diffusion region is reached. However, when $\omega_0 \leq 0.8$, the downward flux is so small within the diffusion region that experimental measurements would be difficult if not impossible.

In general the variation of the upward radiance with angle of observation is much less than that for the downward radiance. The radiance computed from the approximate equations of Van de Hulst has been compared with the exact values. The approximate equations are accurate only when $\omega_0 \geq 0.99$.

The radiance near the lower boundary of an optically thick medium is independent of the solar zenith angle and the azimuthal angle of observation. The variation of the downward and upward radiance as the point of observation is varied from the lower boundary up into the medium is illustrated with examples.

The total downward flux may be greater than unity (normalized to unit incident flux through a plane perpendicular to the solar direction) near the upper boundary when the sun is near the zenith and when ω_0 is near unity. When the medium is absorbing, the downward diffuse flux is greater for Haze L than for Rayleigh phase functions because of the greater forward scattering in the former case.

In the diffusion region the flux (or the radiance at a particular observation angle) decreases as $\exp(-b\tau)$, where b is the attenuation length. The value of b depends only on ω_0 and the phase function. It is always less for Haze L than for Rayleigh scattering for the same value of ω_0 .

The ratio of the upward to the downward flux is remarkably constant within the medium. When $\omega_0 \geq 0.8$, this ratio is constant within 10% for $\tau \geq 3$ down to points near the lower boundary. This ratio is always less for Haze L than for

Rayleigh scattering. When $\omega_0 = 0.5$, the ratio is 0.0171 and 0.132 for Haze L and for Rayleigh scattering respectively; the appreciable difference is due to the backward scattering characteristics of the phase functions.

Within the diffusion region the heating rate is proportional to the total downward flux. The heating rate has its maximum value at an optical depth of two within a Haze L layer when the sun is at the zenith. The optical depth at which this maximum occurs moves toward the top of the haze layer as the solar zenith angle increases and also as the single scattering albedo decreases.

This work was supported in part by Grant No. NGR 44-001-117 from the National Aeronautics and Space Administration. Acknowledgement is made to the National Center for Atmospheric Research, which is sponsored by the National Science Foundation, for computer time used in this research.

REFERENCES

1. G. N. Plass, G. W. Kattawar and F. E. Catchings, Appl. Opt. 12, 314 (1973).
2. G. W. Kattawar and G. N. Plass, JQSRT 13, 1065 (1973).
3. G. N. Plass, G. W. Kattawar and J. Binstock, JQSRT 13, 1081 (1973).
4. G. N. Plass and G. W. Kattawar, Appl. Opt. 8, 455 (1969).
5. G. N. Plass and G. W. Kattawar, J. Phys. Oceanography 2, 139 (1972).
6. G. W. Kattawar and G. N. Plass, J. Phys. Oceanography 2, 146 (1972).
7. R. Bellman, Introduction to Matrix Analysis. McGraw-Hill, New York (1960).
8. D. Deirmendjian, Electromagnetic Scattering on Spherical Polydispersions. American Elsevier, New York (1969).
9. G. W. Kattawar, S. J. Hitzfelder and J. Binstock, J. Atm. Sci. 30, 289 (1973).
10. L. G. Heyney and J. L. Greenstein, Astrophys. J. 93, 70 (1941).
11. G. W. Kattawar, JQSRT 13, 145 (1973).
12. R. W. Preisendorfer, J. Marine Res. 18, 1 (1959).
13. H. C. Van de Hulst, Bull. Astr. Inst. Netherlands 20, 77 (1968).

CAPTIONS FOR FIGURES

FIG. 1. Phase function for single scattering as a function of the cosine of the scattering angle. The real and imaginary part of the index of refraction, n_1 and n_2 , were chosen to be: $n_1 = 1.55$; $n_2 = 0.0$; 0.001 ; 0.0127 ; 0.028 ; 0.23 . The corresponding values of the single scattering albedo $\omega_0 = 1.0$; 0.989 ; 0.890 ; 0.801 ; 0.503 . The average value of the cosine of the scattering angle is: $g = 0.6568$; 0.6682 ; 0.6911 ; 0.7206 ; 0.8326 respectively. The solid curves are calculated from the exact Mie theory and are used in all of the multiple scattering calculations reported here. The approximate Henyey-Greenstein phase function is shown as dashed lines for comparison.

FIG. 2. Downward normalized interior radiance as a function of the cosine (μ) of the zenith angle. Curves are given for various values of the optical depth within a very thick homogeneous layer scattering according to the Haze L phase function for $\omega_0 = 1$. These curves are for $\mu_0 = 0.85332$ (31.42°) and the incident plane containing the direction of the incoming beam ($\phi = 0^\circ$ for left half and $\phi = 180^\circ$ for right half of figure). The solar horizon is at the left of the figure, the zenith is at the center, and the antisolar horizon is at the right of the figure. The incoming flux is normalized to unity across a plane at right angles to the incoming beam. The downward normalized radiance is obtained by multiplying the radiance by the factor (π /diffuse downward flux at optical depth τ).

FIG. 3. Downward normalized interior radiance for $\omega_0 = 0.99$ and $\mu_0 = 0.85332$. See caption to Fig. 2.

FIG. 4. Downward normalized interior radiance for $\omega_0 = 0.9$ and $\mu_0 = 0.85332$. See caption to Fig. 2.

FIG. 5. Downward normalized interior radiance for $\omega_0 = 0.8$ and $\mu_0 = 0.85332$.

See caption to Fig. 2.

FIG. 6. Downward normalized interior radiance for $\omega_0 = 0.5$ and $\mu_0 = 0.85332$.

See caption to Fig. 2.

FIG. 7. Downward normalized interior radiance for $\omega_0 = 0.99$ and $\mu_0 = 0.18816$ (79.15°). See caption to Fig. 2.

FIG. 8. Downward normalized interior radiance for $\omega_0 = 0.5$ and $\mu_0 = 0.18816$.

See caption to Fig. 2.

FIG. 9. Upward and downward normalized interior radiance for $\omega_0 = 1$, $\mu_0 = 0.18817$ (79.15°), and $\mu = 0.26192$ (74.82°) as a function of the azimuthal angle ϕ . The upward normalized radiance is obtained by multiplying the radiance by the factor $(\pi/\text{diffuse upward flux at optical depth } \tau)$.

FIG. 10. Downward normalized interior radiance for $\omega_0 = 0.5$, $\mu_0 = 0.85332$ (31.43°), and $\mu = 0.71392$ (44.45°) as a function of the azimuthal angle ϕ .

FIG. 11. Upward normalized interior radiance for $\omega_0 = 1$ and $\mu_0 = 0.85332$.

The solar horizon is at the left of the figure, the nadir is at center, and the antisolar horizon at the right. The values shown are in the incident plane.

FIG. 12. Upward normalized interior radiance for $\omega_0 = 0.99$ and $\mu_0 = 0.85332$.

FIG. 13. Upward normalized interior radiance for $\omega_0 = 0.8$ and $\mu_0 = 0.85332$.

FIG. 14. Upward normalized interior radiance for $\omega_0 = 0.5$ and $\mu_0 = 0.85332$.

FIG. 15. Upward normalized interior radiance for $\omega_0 = 0.5$ and $\mu_0 = 0.18816$.

FIG. 16. Upward normalized interior radiance for $\omega_0 = 0.5$, $\mu_0 = 0.18816$.

(79.15°), and $\mu = 0.26192$ (74.82°) as a function of azimuthal angle.

FIG. 17. The upward and downward normalized interior radiance in the diffusion region. The solid curves are the exact results from matrix operator theory for $\omega_0 = 0.900$ and Haze L phase function. The dashed curves are calculated from the approximate equation (4). The other quantities are defined in the text.

FIG. 18. The upward and downward normalized interior radiance in the diffusion region for $\omega_0 = 0.80$. See caption to Fig. 17.

FIG. 19. The top set of curves shows the heating rate divided by the total downward flux in the diffusion region as a function of ω_0 . The solid curves are for Rayleigh and the dashed curves for Haze L scattering. The center curves show the diffusion length, b . The lower curves show the quantity $b^2 / 3 (1 - \omega_0)(1 - g)$ which should be constant when the approximate expression given by equation (5) is valid.

FIG. 20. Upward and downward normalized interior radiance for $\omega_0 = 1$ and surface albedo $A = 0$. The optical thickness τ' is measured from the lower surface of an optically deep medium.

FIG. 21. Downward normalized interior radiance for $\omega_0 = 0.8$ and $A = 0$ (lower curves) and $A = 0.15$ (upper curves). The optical thickness τ' is measured from the lower surface of an optically deep medium.

FIG. 22. Upward normalized interior radiance for $\omega_0 = 0.8$ and $A = 0$ (upper curves) and $A = 0.15$ (lower curves). The optical thickness τ' is measured from the lower surface of an optically deep medium.

FIG. 23. Heating rate as a function of the optical depth from the upper boundary of the medium for $\omega_0 = 0.99$. Curves are shown for $\mu_0 = 1.0$; 0.85332; 0.53786; 0.40452; 0.18816. All curves are normalized to the value unity at $\tau = 0$.

FIG. 24. Heating rate as a function of the optical depth from the upper boundary of the medium for $\mu_0 = 1.0$ and 0.18816 . Curves are shown for $\omega_0 = 0.99$; 0.9 ; 0.8 ; 0.5 . All curves are normalized to the value unity at $\tau = 0$.

TABLE 1

ω_0	$I^{\text{up}}(1)/I^{\text{up}}(0.03785)$		$I^{\text{down}}(1)/I^{\text{down}}(0.03785)$		b	
	Rayleigh	Haze L	Rayleigh	Haze L	Rayleigh	Haze L
0.99	0.8614	0.7647	1.2045	1.3542	0.1724	0.1011
0.9	0.6939	0.4594	2.1305	3.0411	0.5232	0.3119
0.8		0.3406		5.684	0.7048	0.4363
0.5	~0.68	0.1616	~17	46.6	0.9474	0.676
0.1	~0.94		~66		0.999853	

TABLE 2

$$\omega_0 = 1, \mu_0 = 1$$

Optical Depth	F^{up}	$F^{\text{down}}_{\text{diffuse}}$	$F^{\text{down}}_{\text{total}}$	$F^{\text{down}}_{\text{total}} - F^{\text{up}}$	$I^{\text{up}}(1)/I^{\text{up}}(0.03785)$	$I^{\text{down}}(1)/I^{\text{down}}(0.03785)$
0	0.9997	0	1.0000	2.95 -4	2.36198	
0.125	1.0278	0.1456	1.0281	2.95 -4	1.95681	1.54712
0.25	1.0511	0.2726	1.0514	2.95 -4	1.76265	2.30160
0.5	1.0896	0.4834	1.0899	2.95 -4	1.53524	3.09905
1	1.1462	0.7786	1.1465	2.95 -4	1.30710	3.37610
5	1.2660	1.2596	1.2663	2.95 -4	1.01172	1.23649
13	1.2720	1.2723	1.2723	2.95 -4	0.99986	1.00066
77	1.2672	1.2675	1.2675	2.95 -4	0.99983	1.00017
205	1.2575	1.2578	1.2578	2.95 -4	0.99983	1.00017
8,397	0.6360	0.6363	0.6363	2.94 -4	0.99966	1.00033
16,589	1.553 -2	1.583 -2	1.583 -2	2.94 -4	0.98645	1.01353
16,717	5.841 -3	6.135 -3	6.135 -3	2.94 -4	0.96450	1.03540
16,781	9.948 -4	1.289 -3	1.289 -3	2.94 -4	0.81270	1.18459
16,789	3.890 -4	6.830 -4	6.830 -4	2.94 -4	0.60117	1.39046
16,793	8.329 -5	3.774 -4	3.774 -4	2.94 -4	0.20368	1.94359
16,793.5	4.330 -5	3.374 -4	3.374 -4	2.94 -4	0.11370	2.20911
16,793.875	1.161 -5	3.057 -4	3.057 -4	2.94 -4	0.03545	2.66501
16,794	0	2.941 -4	2.941 -4	2.94 -4		3.11798

TABLE 3

$$\omega_0 = 0.99 \quad \mu_0 = 1$$

Optical Depth	F^{up}	$F^{down}_{diffuse}$	F^{down}_{total}	F^{up}/F^{down}_{total}	$\frac{\partial F}{\partial t}$	$I^{up}(1)/I^{up}(0.03785)$	$I^{down}(1)/I^{down}(0.03785)$
0	0.6089	0	1.0000	0.609		2.11853	
0.000977	0.6090	1.088-3	1.0001	0.609	2.118-2	2.11312	0.93211
0.00293	0.6093	3.259-3	1.0003	0.609	2.123-2	2.10254	0.95027
0.01074	0.6103	1.188-2	1.0012	0.610	2.142-2	2.06304	1.02449
0.04199	0.6141	4.543-2	1.0043	0.611	2.207-2	1.93816	1.34141
0.1045	0.6207	0.1086	1.0094	0.615	2.303-2	1.77228	2.01130
0.4795	0.6458	0.4062	1.0252	0.630	2.639-2	1.33131	4.40245
0.9795	0.6583	0.6484	1.0239	0.643	2.870-2	1.09712	4.92285
2.98	0.6079	0.8634	0.9142	0.664	2.904-2	0.83326	2.94923
8.98	0.3463	0.5148	0.5150	0.673	1.703-2	0.76594	1.38913
16.98	0.1544	0.2295	0.2295	0.673	7.595-3	0.76474	1.35437
24.98	6.874-2	0.1022	0.1022	0.673	3.382-3	0.76474	1.35423
32.98	3.061-2	4.551-2	4.551-2	0.673	1.506-3	0.76474	1.35423
40.98	1.363-2	2.027-2	2.027-2	0.673	6.708-4	0.76474	1.35423
52.98	4.051-3	6.023-3	6.023-3	0.673	1.994-5	0.76473	1.35423
68.98	8.032-4	1.194-3	1.194-3	0.672	3.953-5	0.76462	1.35434
84.98	1.581-4	2.361-4	2.361-4	0.670	7.801-6	0.76165	1.35718
92.98	6.825-5	1.037-4	1.037-4	0.658	3.402-6	0.74883	1.39942
100.98	2.552-5	4.289-5	4.289-5	0.595	1.354-6	0.67492	1.43974
108.98	0	1.135-5	1.135-5	0.000	1.925-7		3.26020

30A

TABLE 4

$$\omega_0 = 0.9 \quad \mu_0 = 1$$

Optical Depth	F^{up}	$F^{\text{down}}_{\text{diffuse}}$	$F^{\text{down}}_{\text{total}}$	$F^{\text{up}}/F^{\text{down}}_{\text{total}}$	$\frac{\partial F}{\partial t}$	$I^{\text{up}}(1)/I^{\text{up}}(0.03783)$	$I^{\text{down}}(1)/I^{\text{down}}(0.03785)$
0	0.2022	0	1.0000	0.202		1.65111	
0.000977	0.2023	8.664-4	0.9999	0.202	0.1391	1.64672	2.03001
0.00239	0.2023	2.595-3	0.9997	0.202	0.1393	1.63812	2.06993
0.01074	0.2025	9.459-3	0.9988	0.203	0.1401	1.60595	2.23310
0.04199	0.2032	3.613-2	0.9950	0.204	0.1426	1.50348	2.93144
0.1045	0.2040	8.605-2	0.9868	0.207	0.1460	1.36536	4.41680
0.2295	0.2046	0.1740	0.9689	0.211	0.1501	1.19169	6.99678
0.4795	0.2031	0.3102	0.9293	0.218	0.1539	0.99044	9.95307
0.9795	0.1934	0.4671	0.8426	0.230	0.1526	0.78746	11.63538
2.98	0.1291	0.4622	0.5130	0.252	0.1084	0.54596	8.15446
8.98	2.248-2	8.507-2	8.520-2	0.264	1.945-2	0.46348	3.37065
16.98	1.868-3	7.060-3	7.060-3	0.265	1.619-3	0.45943	3.04697
24.98	1.541-4	5.824-4	5.824-4	0.265	1.336-4	0.45935	3.04117
32.98	1.271-5	4.804-5	4.804-5	0.265	1.102-5	0.45935	3.04107
40.98	1.049-6	3.963-6	3.963-6	0.265	9.088-7	0.45935	3.04107
48.98	8.650-8	3.268-7	3.268-7	0.265	7.496-8	0.45935	3.04107
56.98	7.135-9	2.696-8	2.696-8	0.265	6.184-9	0.45935	3.04107
64.98	5.992-10	2.224-9	2.224-9	0.265	5.100-10	0.45899	3.04138
72.98	4.503-11	1.825-10	1.825-10	0.247	4.126-11	0.40989	3.08872
76.98	0	4.854-11	4.854-11	-.000	7.800-12		4.87874

TABLE 5

$$\omega_0 = 0.8, \mu_0 = 1$$

Optical Depth	F^{up}	$F^{\text{down}}_{\text{diffuse}}$	$F^{\text{down}}_{\text{total}}$	$F^{\text{up}}/F^{\text{down}}_{\text{total}}$	$\frac{\partial F}{\partial \tau}$	$I^{\text{up}}(1)/I^{\text{up}}(0.03785)$	$I^{\text{down}}(1)/I^{\text{down}}(0.03785)$
0	9.597 -2	0	1.0000	0.096		1.25515	
0.000977	9.597 -2	7.484 -4	0.9998	0.096	0.2390	1.25195	3.18154
0.00293	9.598 -2	2.242 -3	0.9993	0.096	0.2392	1.24568	3.24521
0.01074	9.602 -2	8.167 -3	0.9975	0.096	0.2399	1.22221	3.50578
0.04199	9.610 -2	3.115 -2	0.9900	0.097	0.2420	1.14735	4.62678
0.1045	9.602 -2	7.396 -2	0.9747	0.098	0.2443	1.04618	7.04223
0.2295	9.530 -2	0.1484	0.9434	0.101	0.2453	0.91838	11.35469
0.4795	9.251 -2	0.2605	0.8796	0.105	0.2417	0.76901	16.62676
0.9795	8.413 -2	0.3790	0.7545	0.111	0.2236	0.61584	20.39000
2.98	4.605 -2	0.3175	0.3683	0.125	0.1158	0.42465	16.41225
8.98	4.076 -3	3.017 -2	3.029 -2	0.134	1.131 -2	0.34725	6.93749
16.98	1.269 -4	9.360 -4	9.360 -4	0.136	3.528 -4	0.34086	5.73525
24.98	3.874 -6	2.856 -5	2.856 -5	0.136	1.077 -5	0.34059	5.68608
32.98	1.182 -7	8.711 -7	8.711 -7	0.136	3.285 -7	0.34058	5.68421
40.98	3.603 -9	2.657 -8	2.657 -8	0.136	1.002 -8	0.34058	5.68414
48.98	1.099 -10	8.103 -10	8.103 -10	0.136	3.056 -10	0.34058	5.68414
56.98	3.352 -12	2.471 -11	2.471 -11	0.136	9.319 -12	0.34058	5.68414
64.98	1.022 -13	7.537 -13	7.537 -13	0.136	2.842 -13	0.34056	5.68416
72.98	3.043 -15	2.298 -14	2.298 -14	0.132	8.640 -15	0.32414	5.70033
76.98	0	3.919 -15	3.919 -15	0.000	1.190 -15		7.75191

TABLE 6

$$\omega_o = 0.5, \mu_o = 1$$

Optical Depth	F^{up}	$F^{down}_{diffuse}$	F^{down}_{total}	F^{up}/F^{down}_{total}	$\frac{\partial F}{\partial \tau}$	$I^{up}(1)/I^{up}(0.03785)$	$I^{down}(1)/I^{down}(0.03785)$
0	1.136 -2	0	1.0000	1.14 -2		0.36251	
0.000977	1.136 -2	4.717 -4	0.9995	1.14 -2	0.5136	0.36187	12.1281
0.00293	1.135 -2	1.413 -3	0.9985	1.14 -2	0.5133	0.36063	12.3863
0.01074	1.133 -2	5.144 -3	0.9944	1.14 -2	0.5120	0.35599	13.4484
0.04199	1.123 -2	1.957 -2	0.9784	1.15 -2	0.5065	0.34151	18.1146
0.1045	1.101 -2	4.616 -2	0.9469	1.16 -2	0.4943	0.32272	28.7095
0.2295	1.053 -2	9.133 -2	0.8863	1.19 -2	0.4687	0.29981	49.7497
0.4795	9.526 -3	0.1554	0.7745	1.23 -2	0.4181	0.27307	81.4235
0.9795	7.601 -3	0.2115	0.5870	1.29 -2	0.3268	0.24429	117.3569
2.98	2.639 -3	0.1305	0.1814	1.46 -2	0.1085	0.20060	139.3654
8.98	6.499 -5	3.841 -3	3.967 -3	1.63 -2	2.562 -3	0.17052	80.9573
16.98	3.260 -7	1.918 -5	1.922 -5	1.70 -2	1.270 -5	0.16322	53.0714
24.98	1.495 -9	8.755 -8	8.756 -8	1.71 -8	5.810 -8	0.16188	47.7130
32.98	6.736 -12	3.941 -10	3.941 -10	1.71 -2	2.617 -10	0.16163	46.7685
40.98	3.026 -14	1.770 -12	1.770 -12	1.71 -2	1.176 -12	0.16158	46.6074
48.98	1.359 -16	7.948 -15	7.948 -15	1.71 -2	5.279 -15	0.16158	46.5803
56.98	6.100 -19	3.568 -17	3.568 -17	1.71 -2	2.370 -17	0.16157	46.5757
60.98	4.078 -20	2.391 -18	2.391 -18	1.71 -2	1.588 -18	0.16032	46.5769
64.98	0	1.601 -19	1.601 -19	0.000	1.022 -18		52.1052

33
A

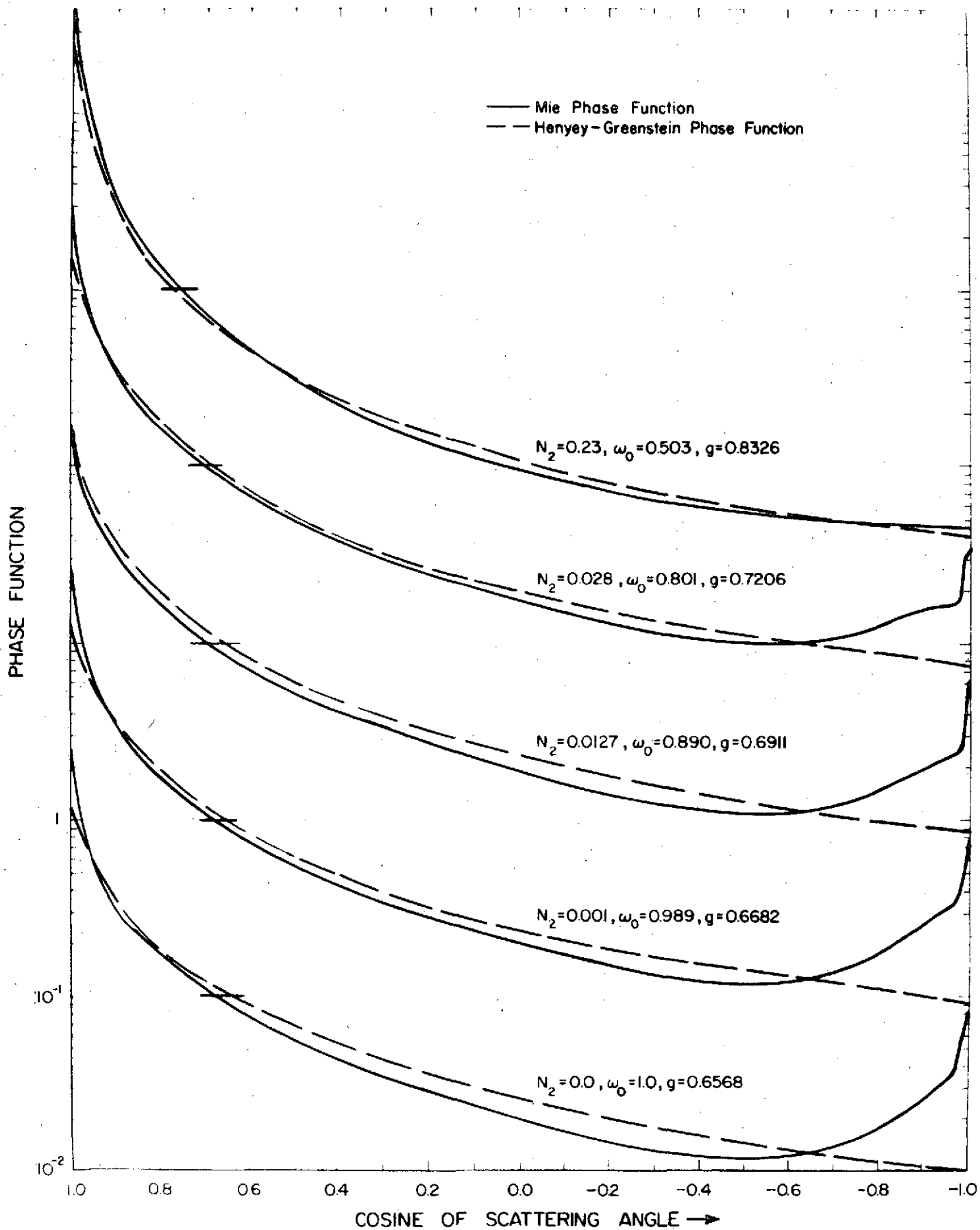
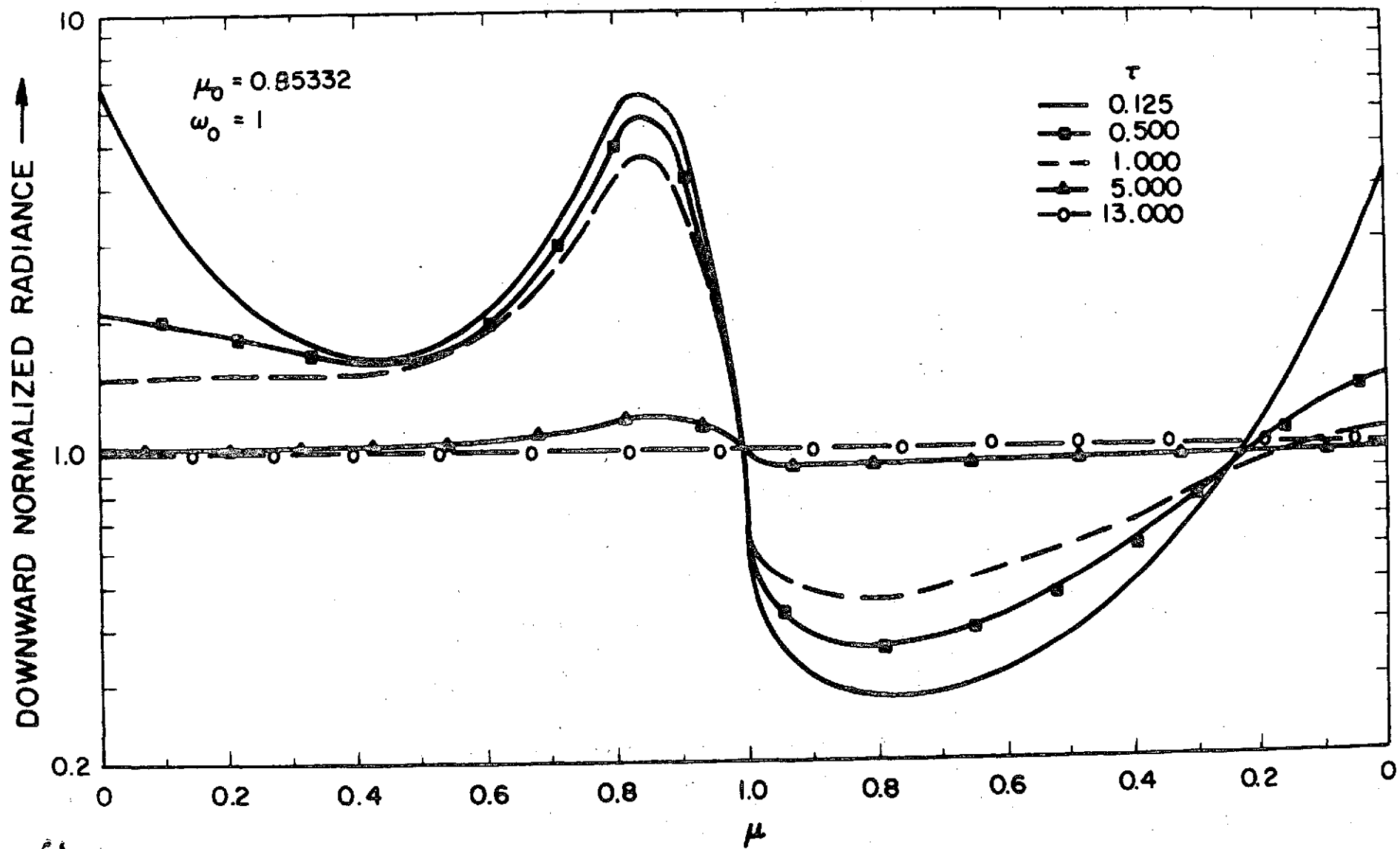
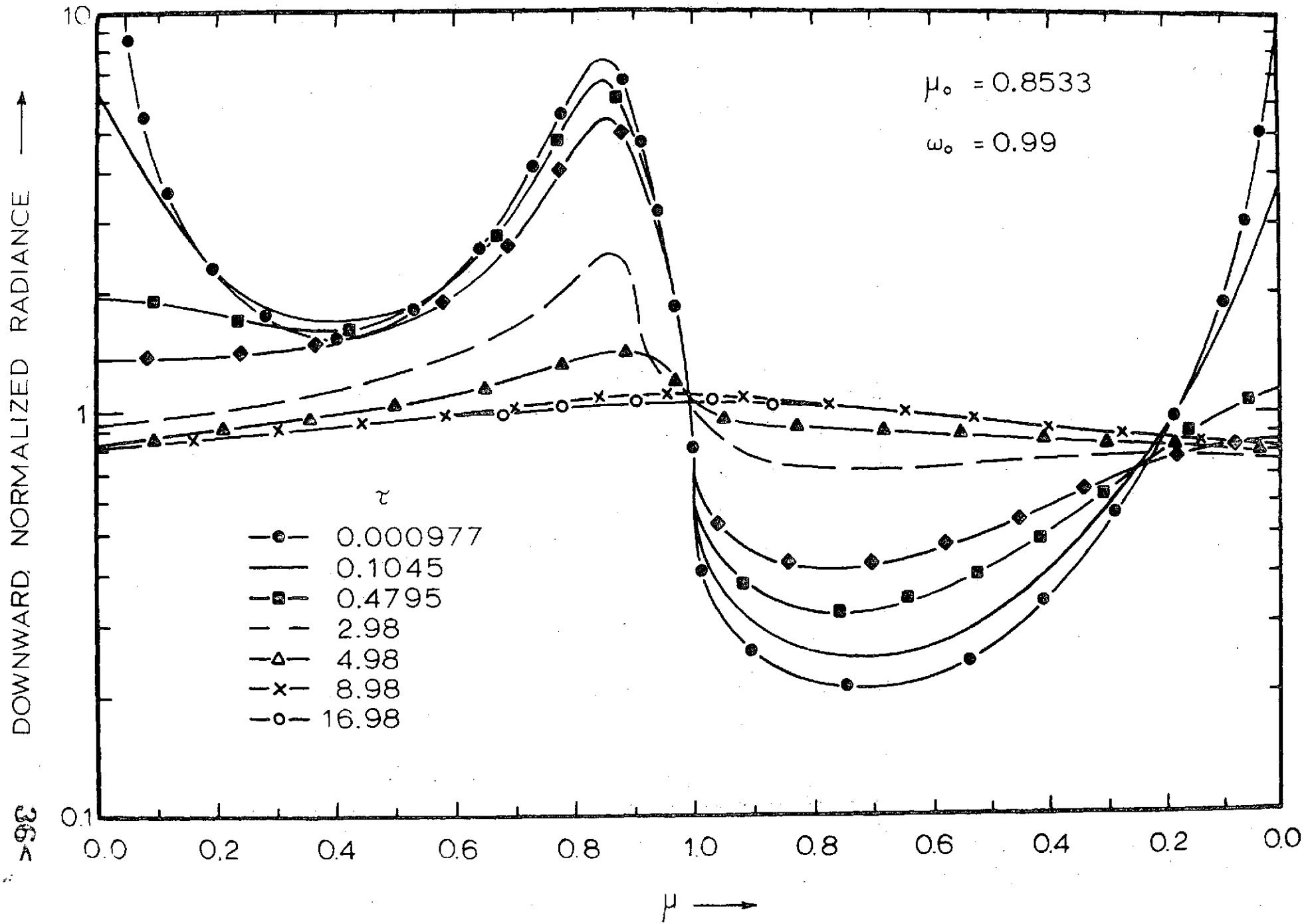


Fig. 1





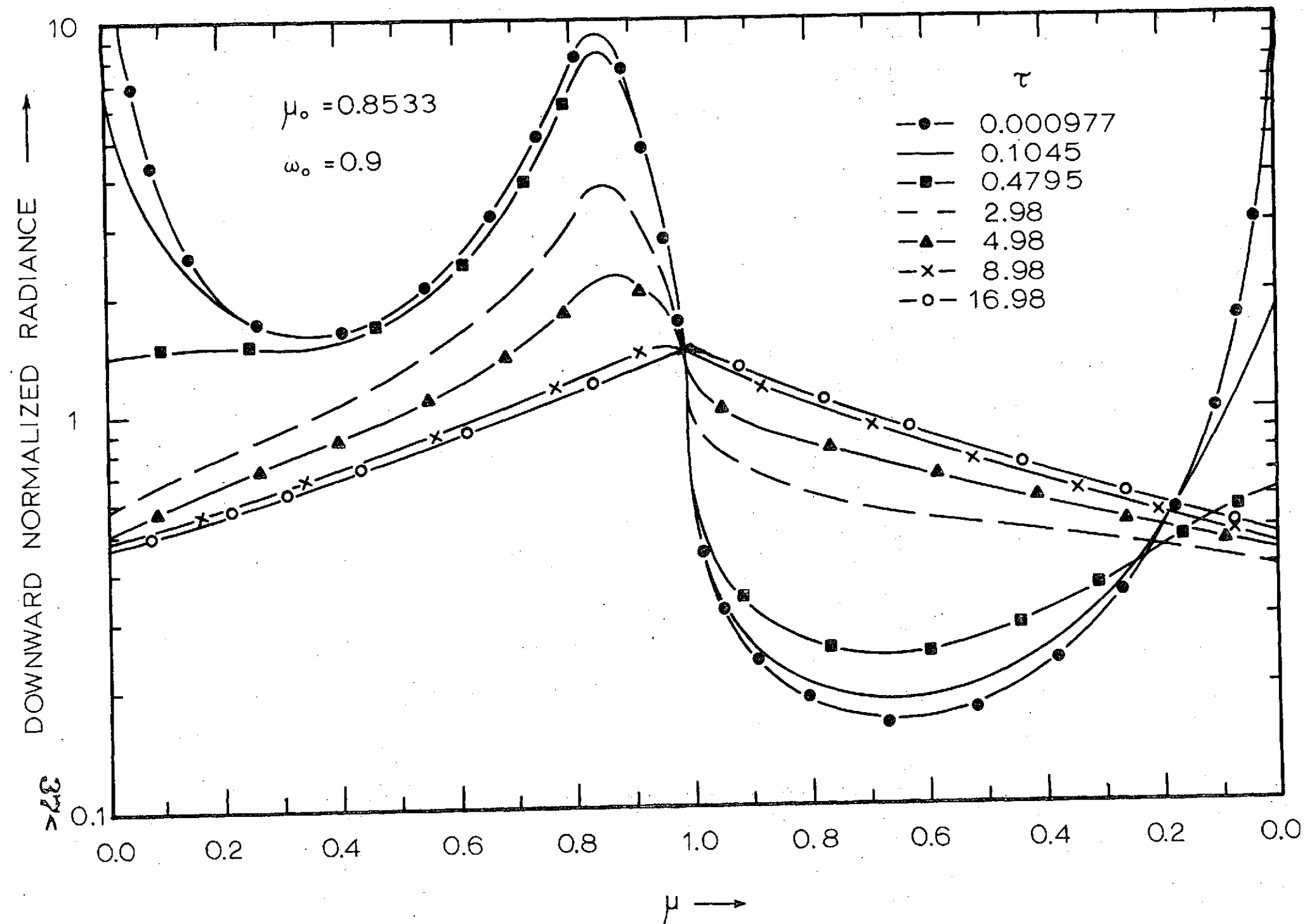


Fig. 4

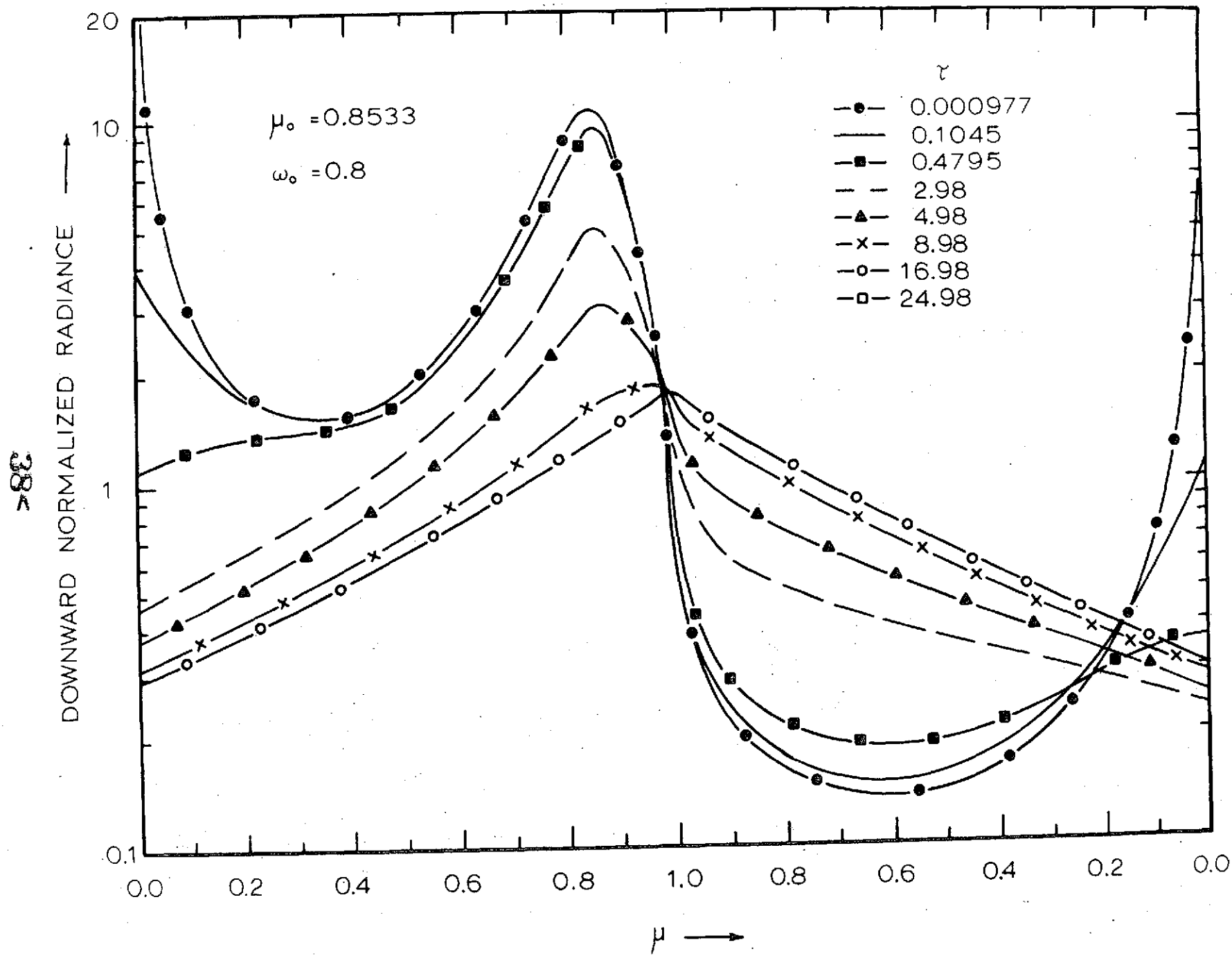
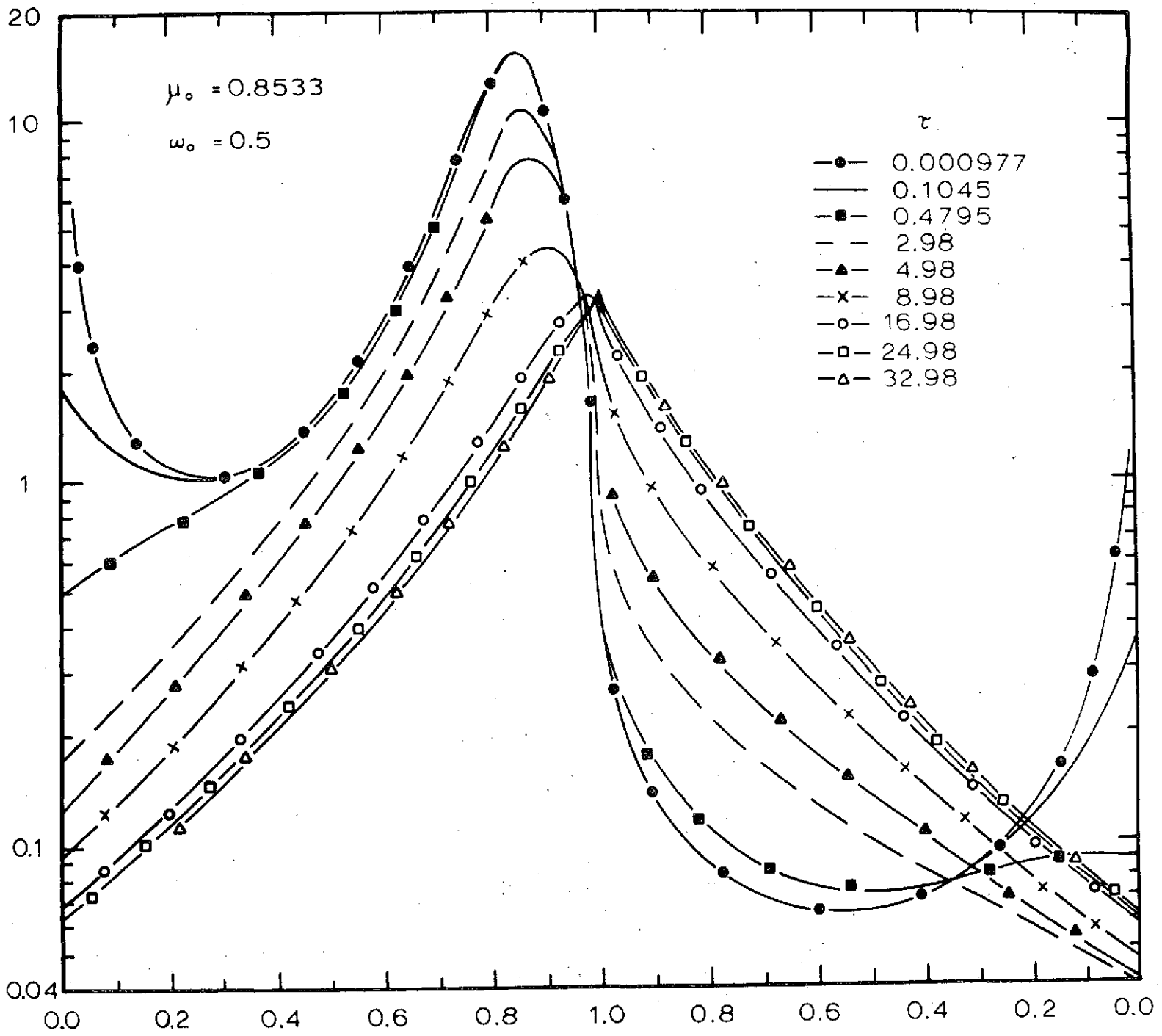


Fig. 5

DOWNWARD NORMALIZED RADIANCE



μ
Fig. 6

707

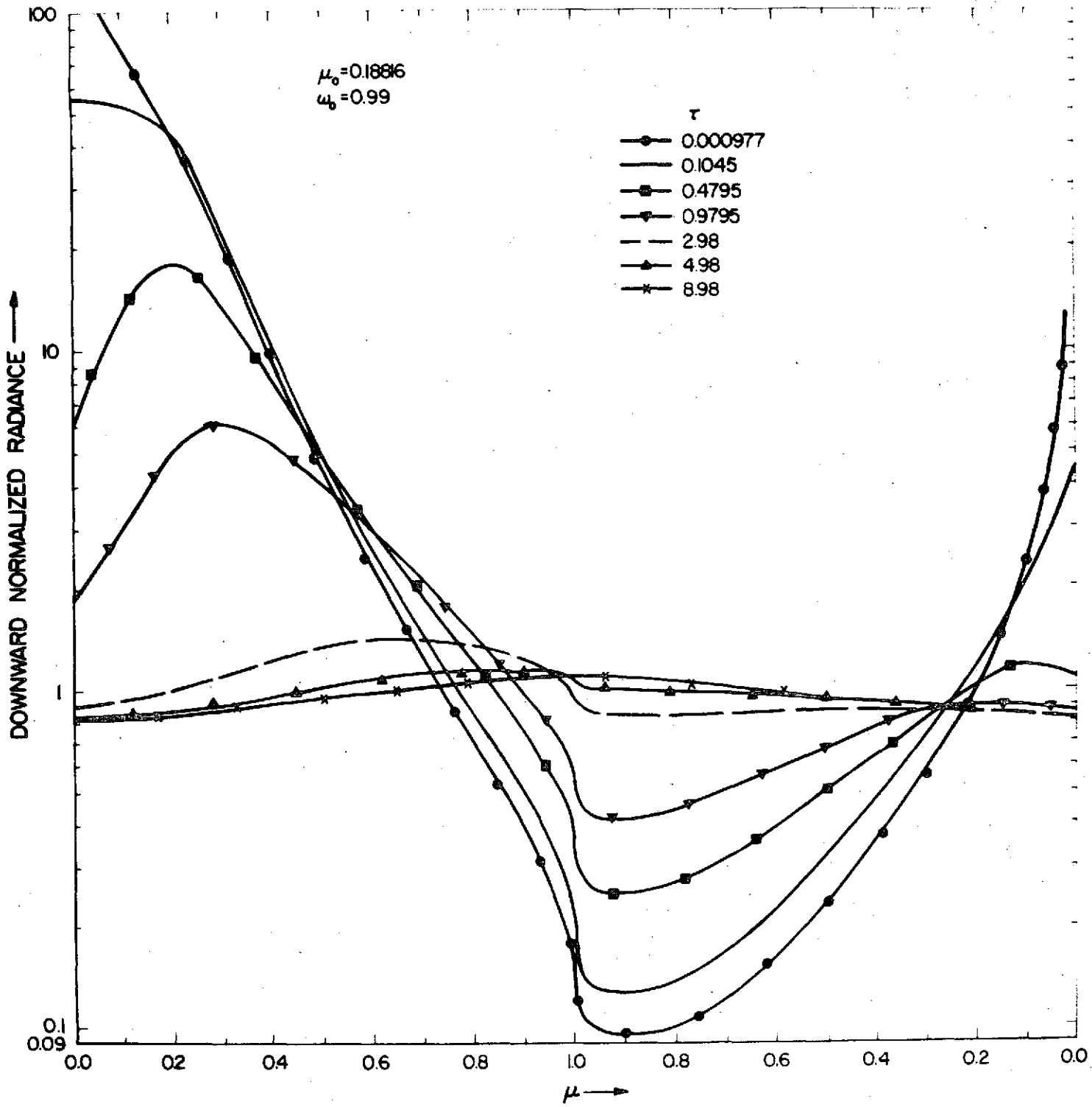
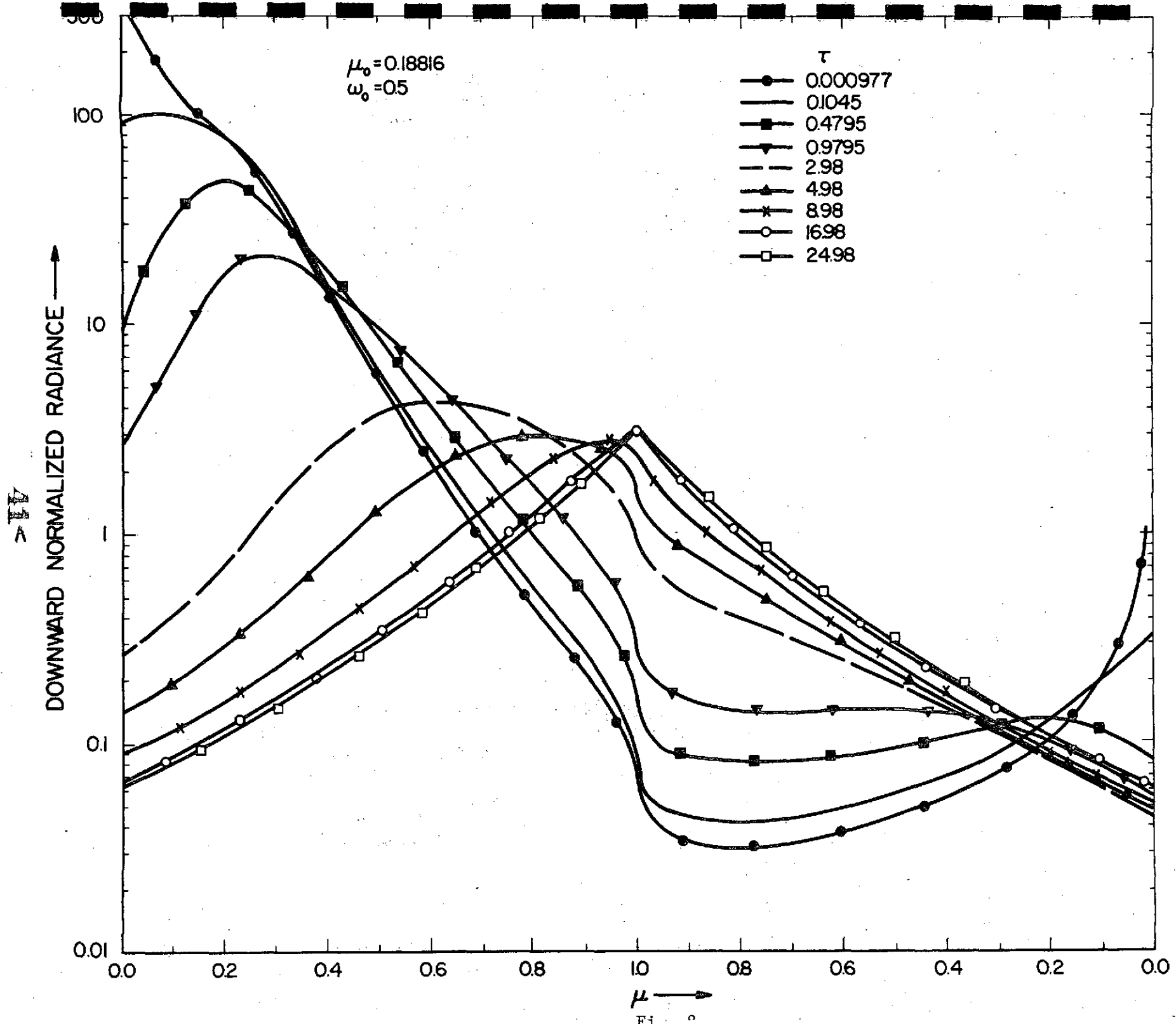


Fig. 7



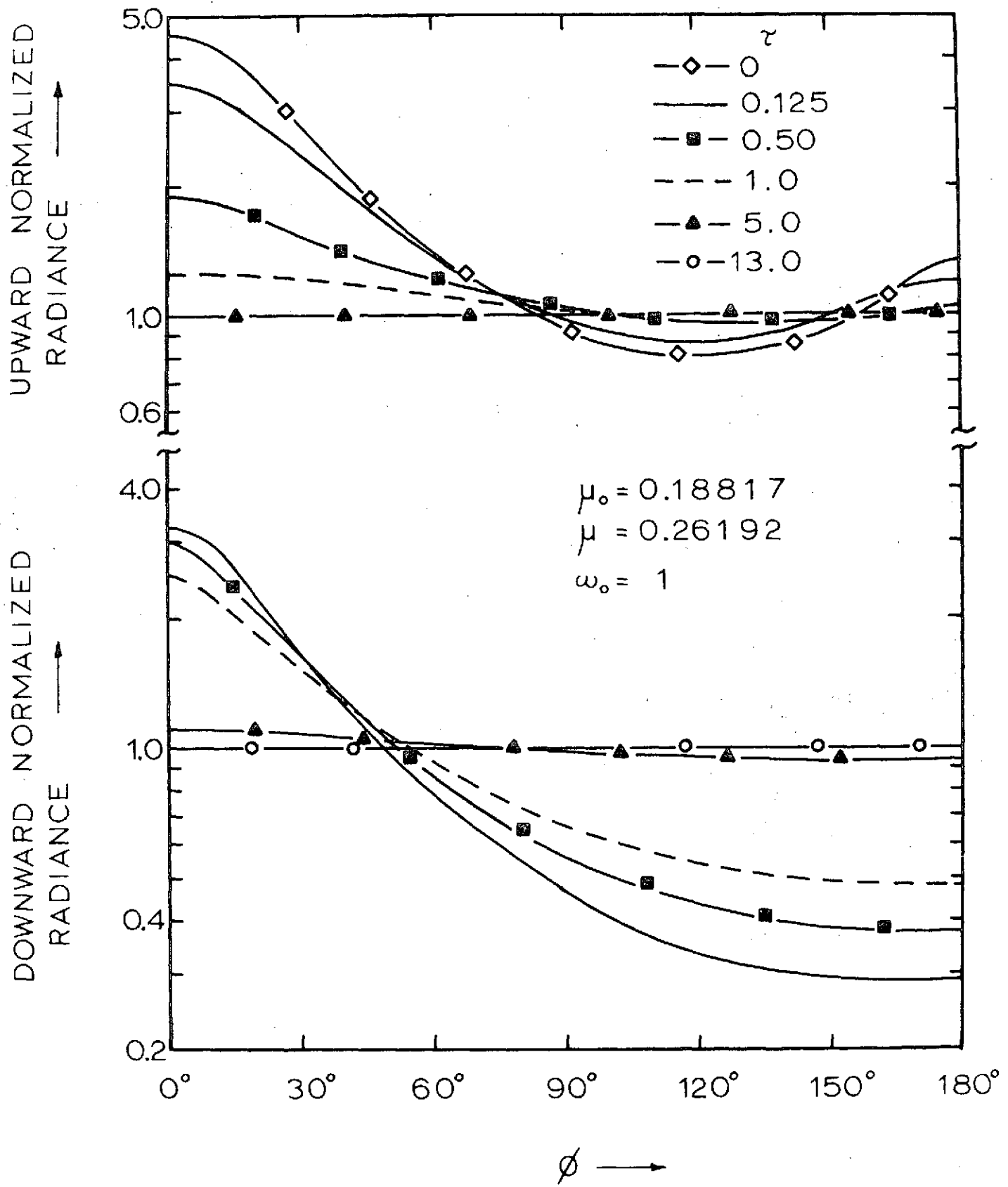


Fig. 9

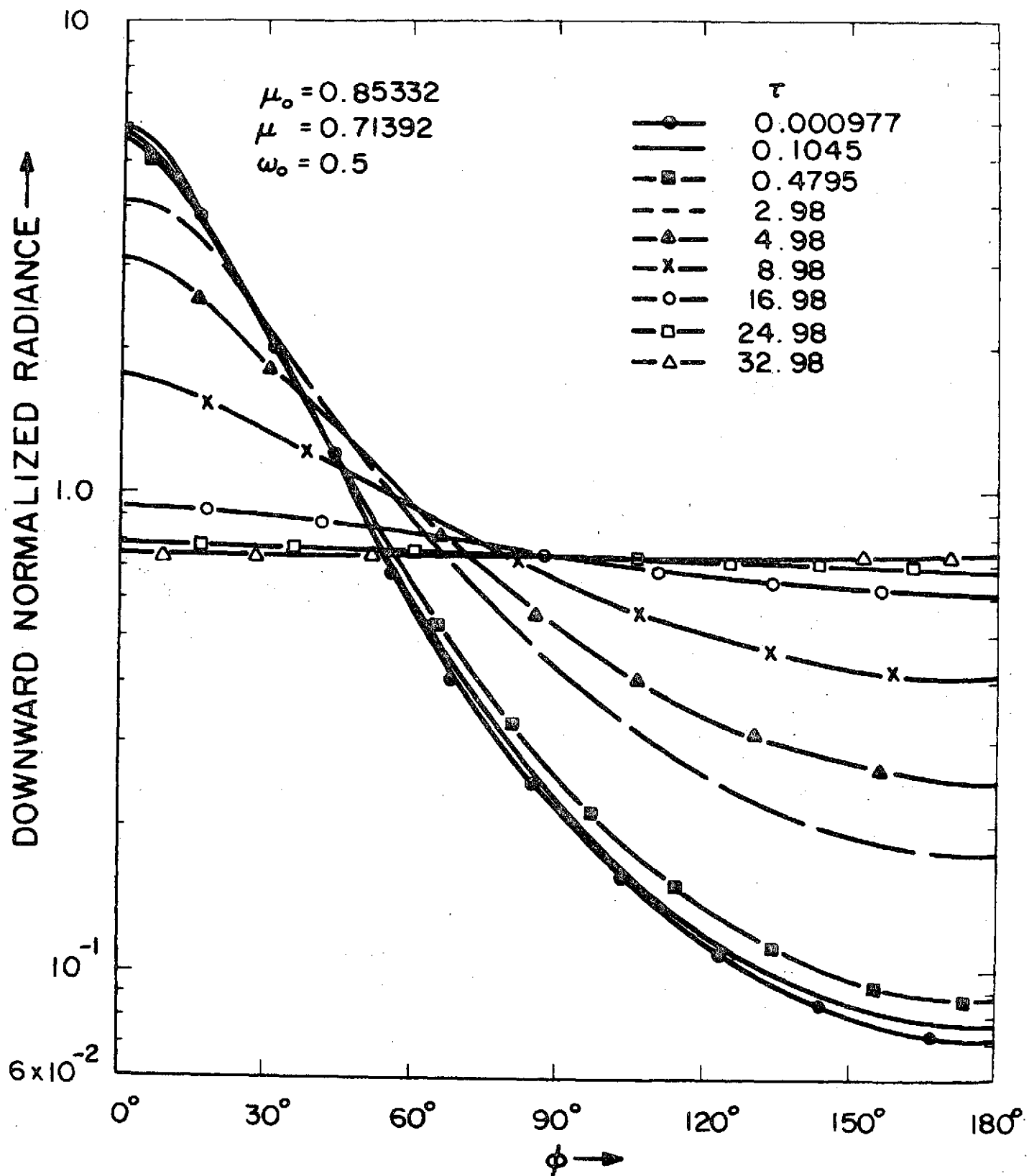


Fig. 10

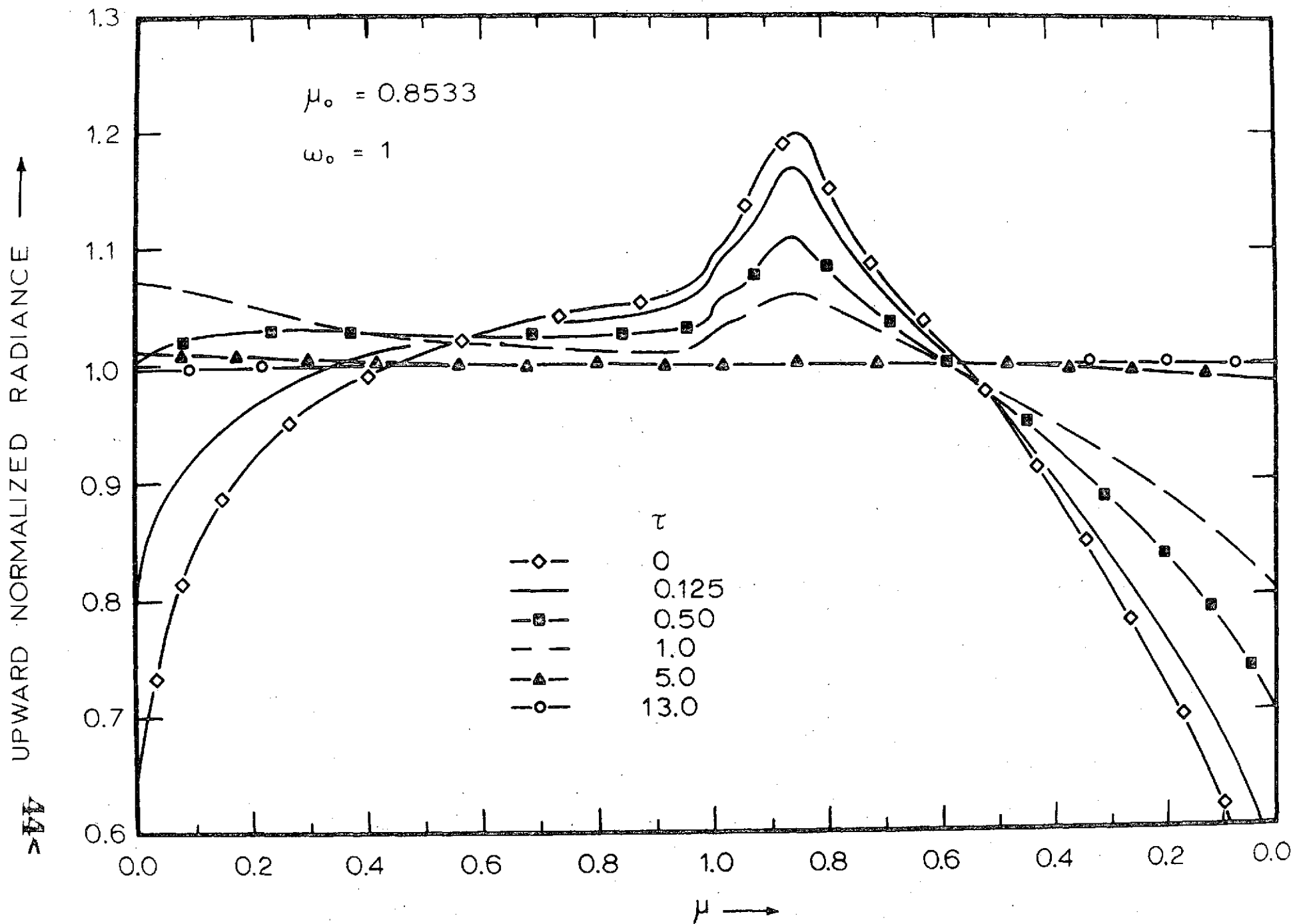


FIG. 11

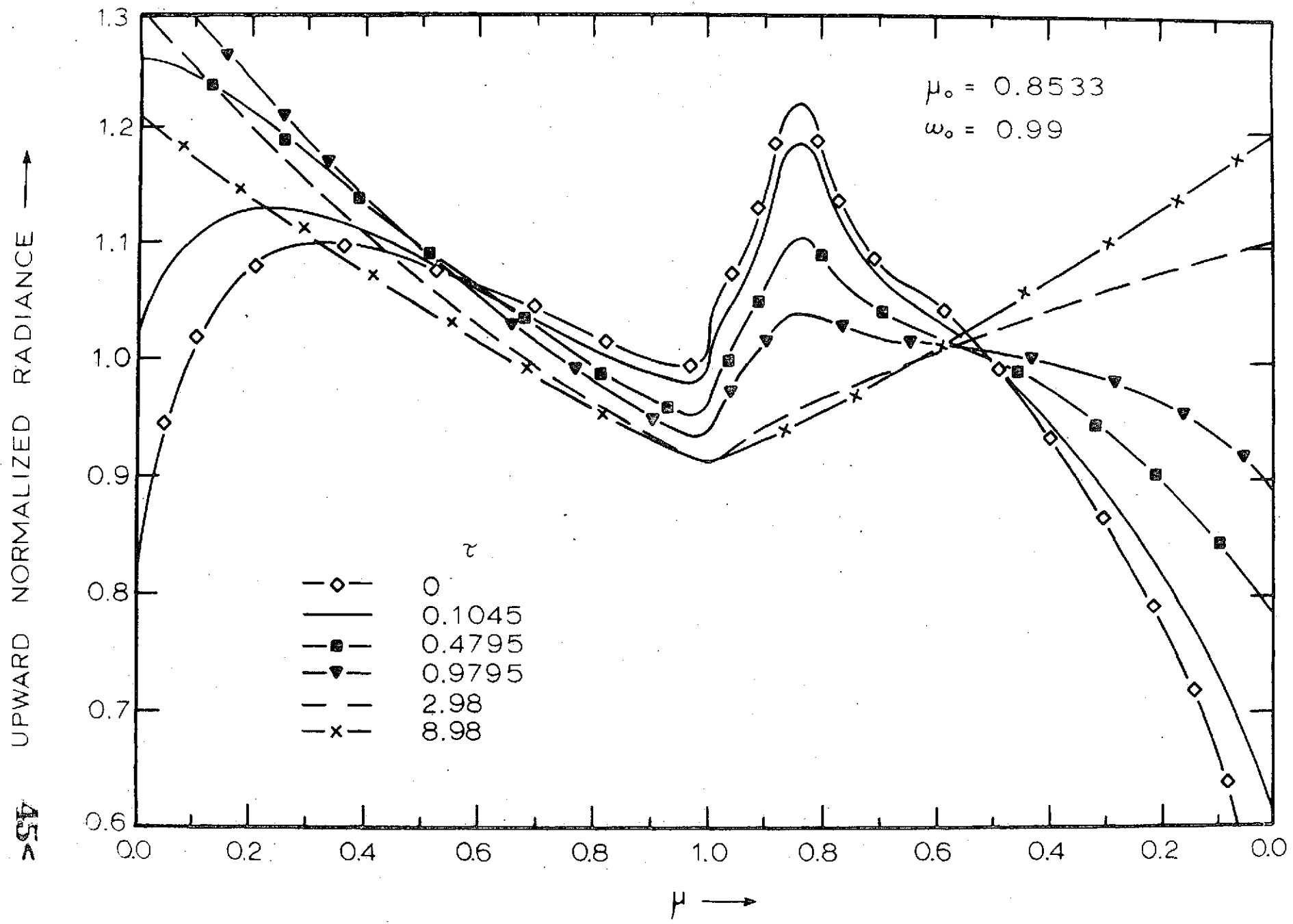


Fig. 12

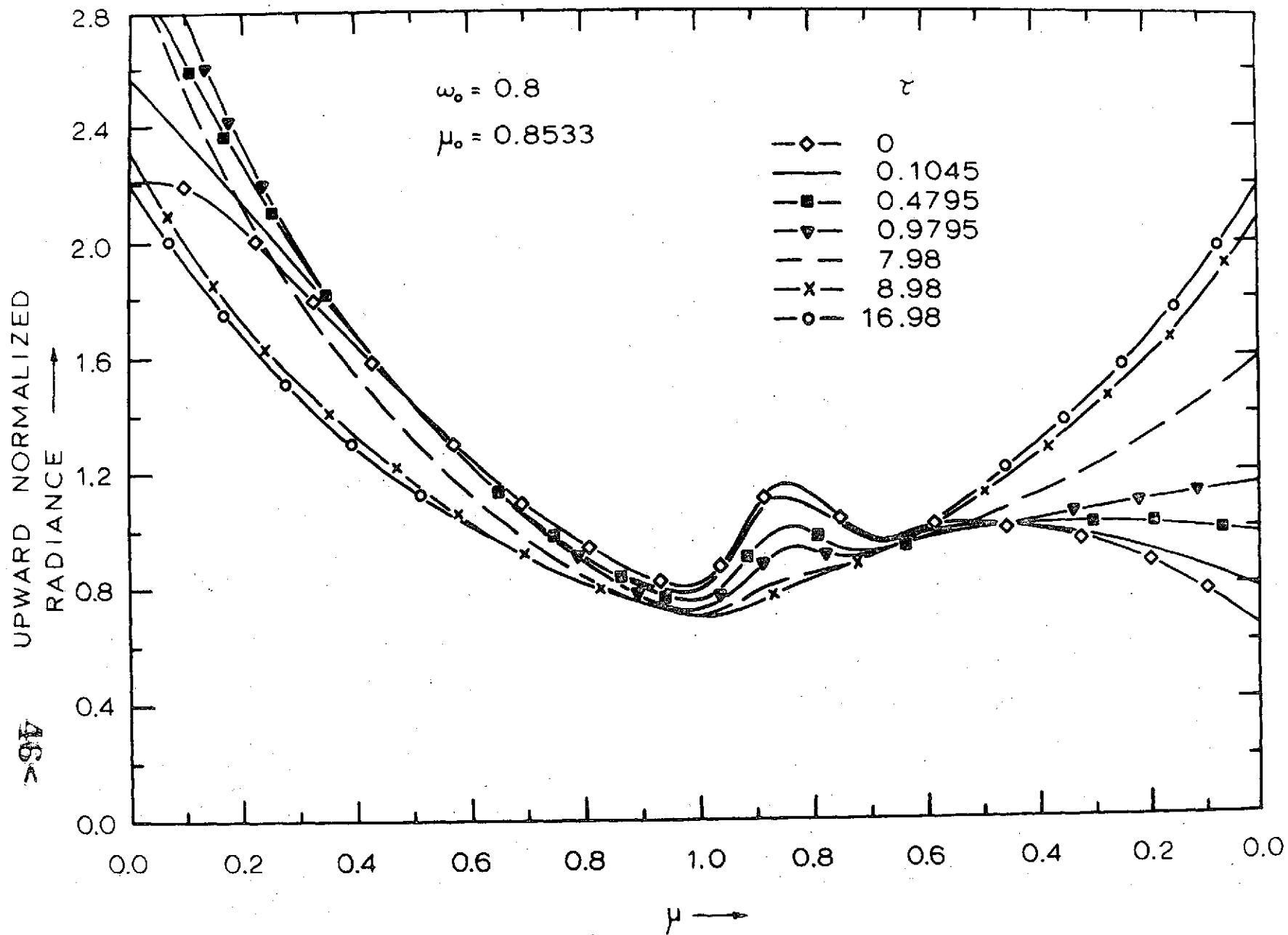


Fig. 13

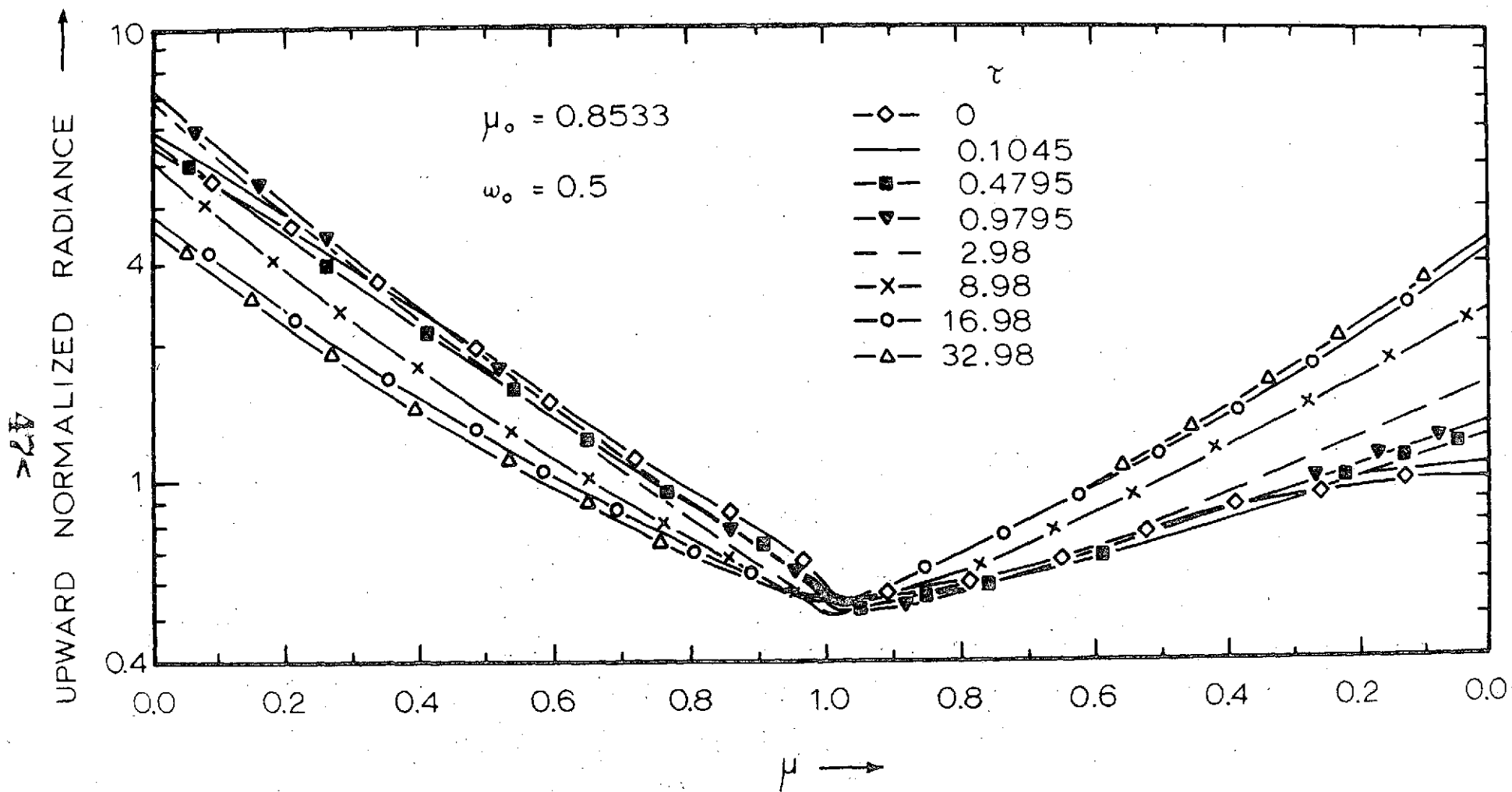


Fig. 14

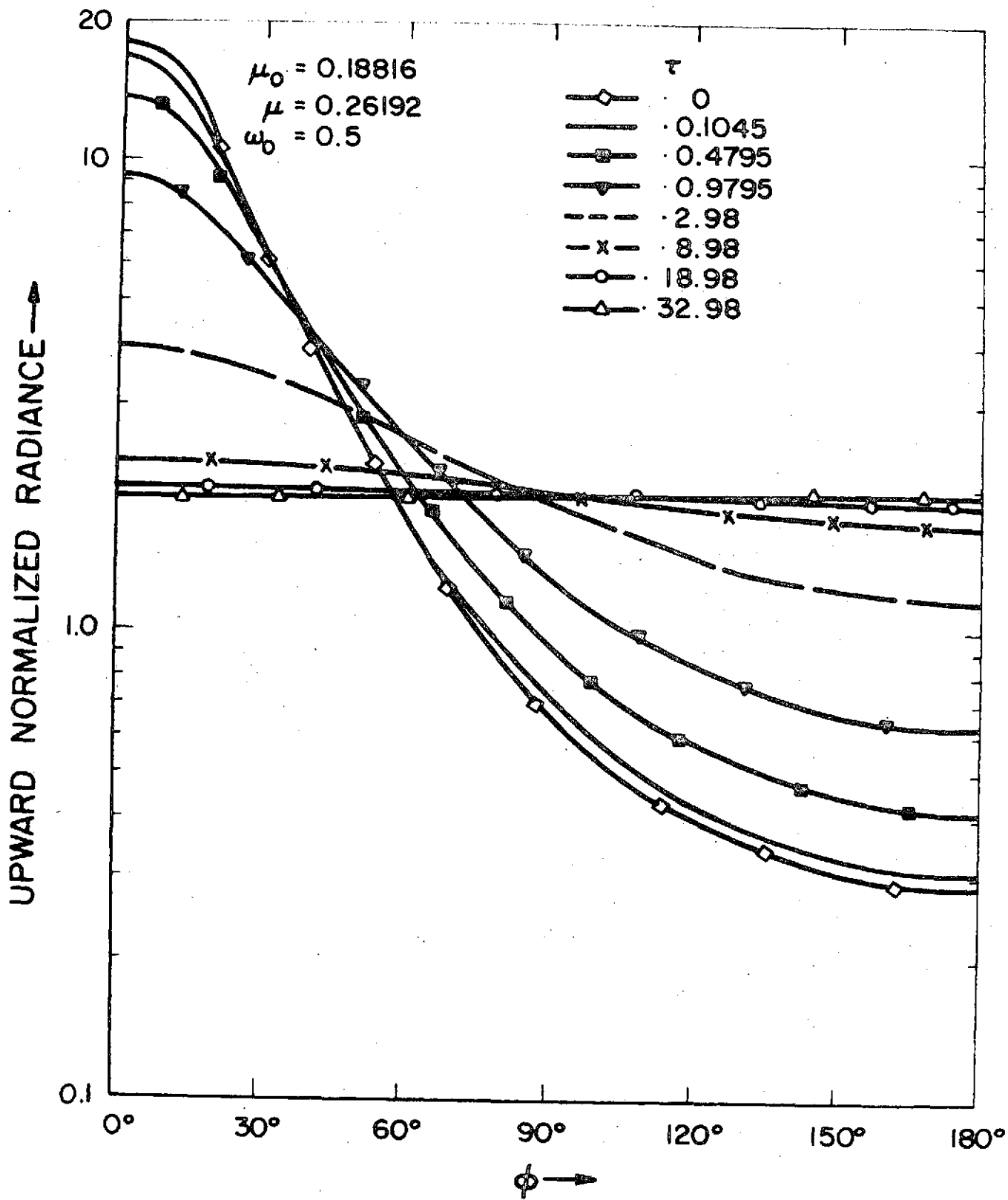
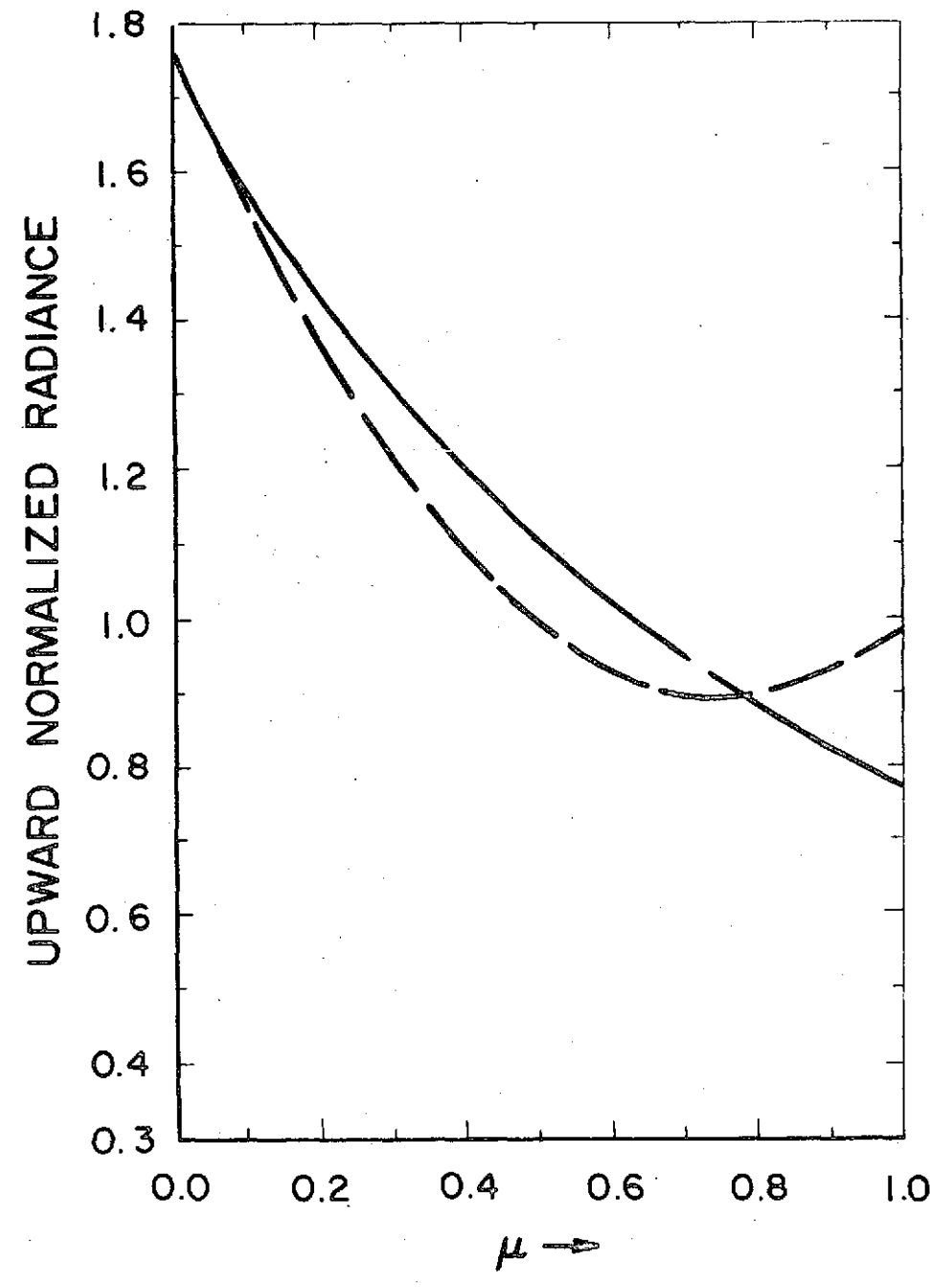
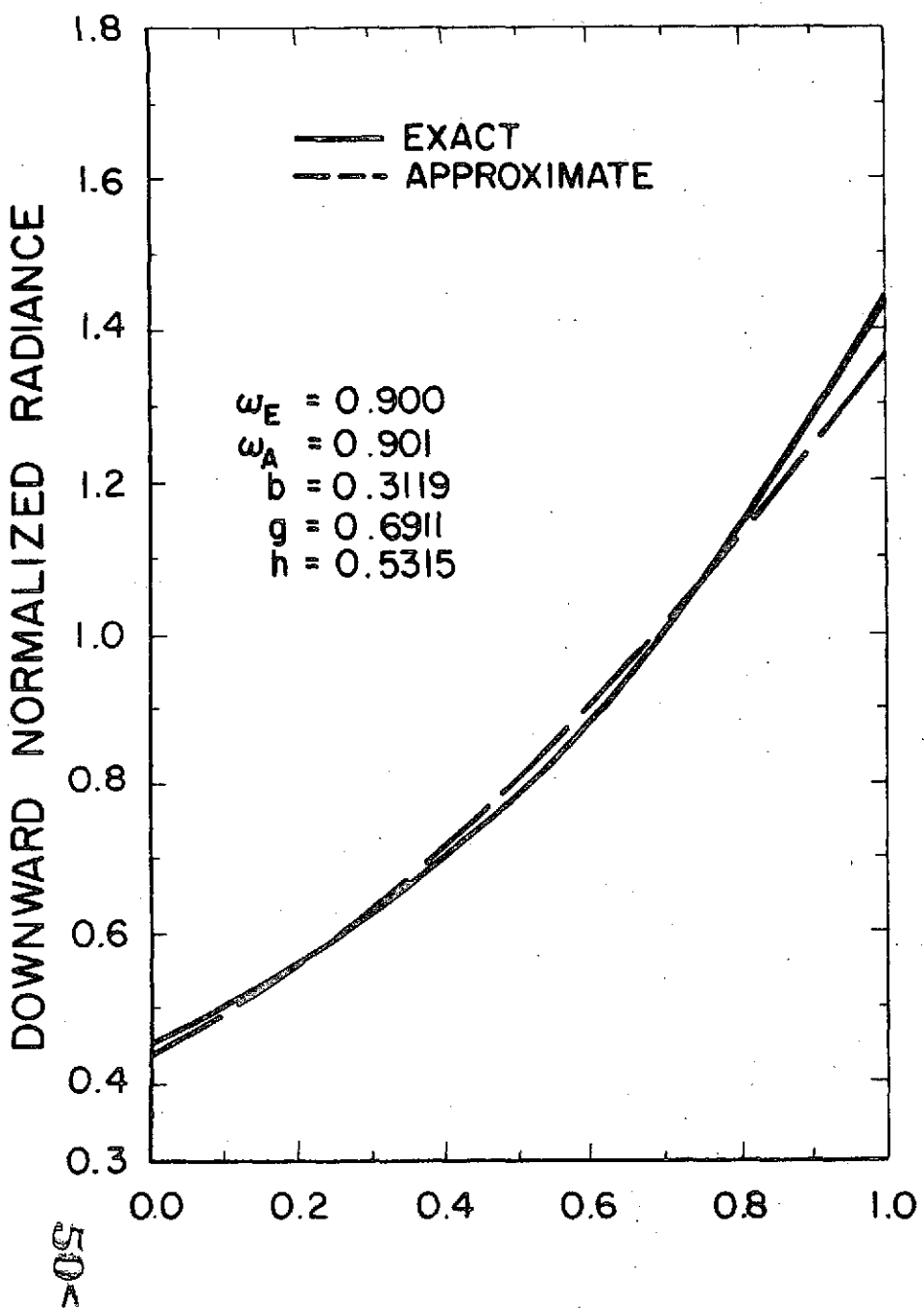


Fig. 16



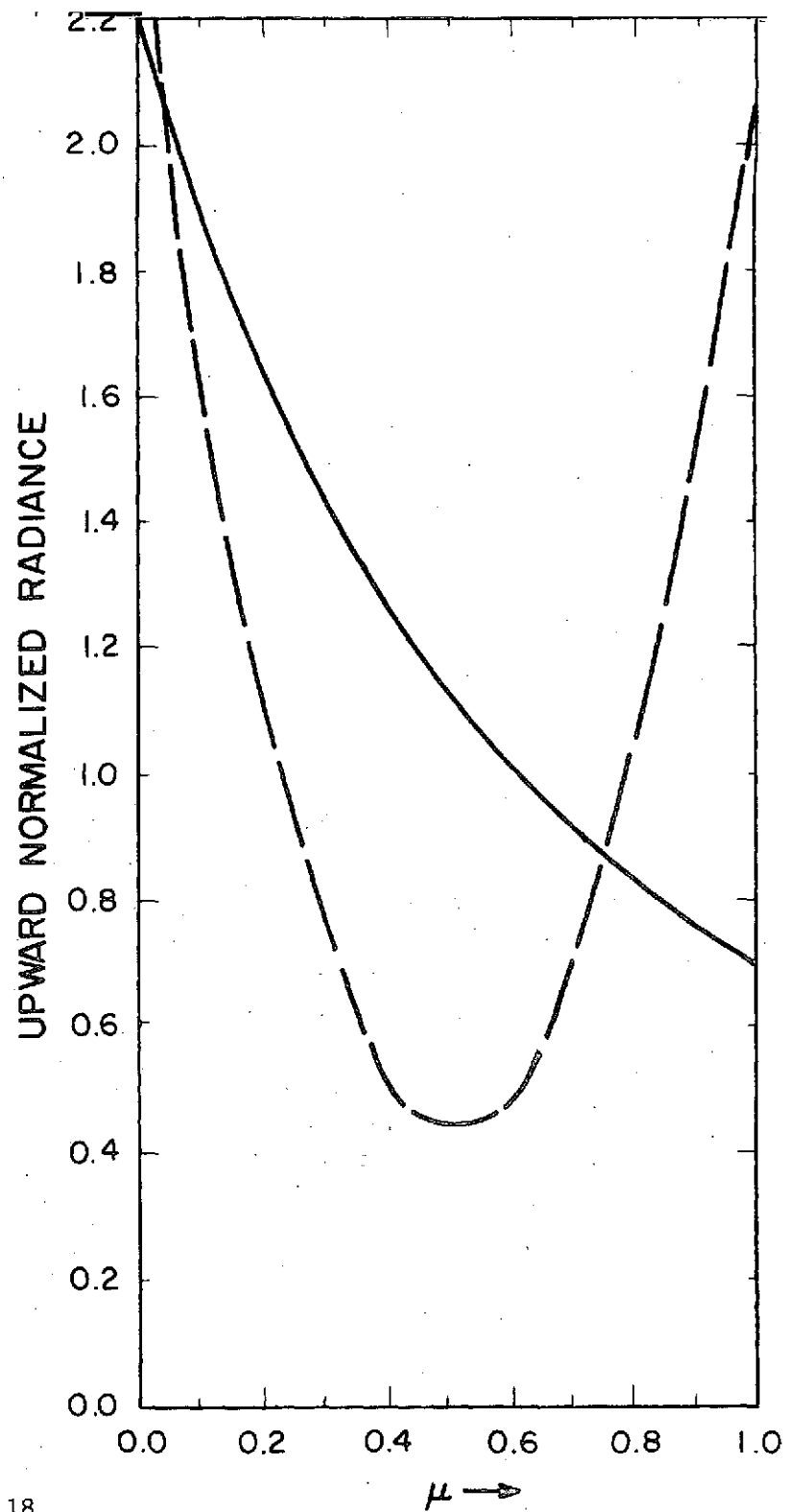
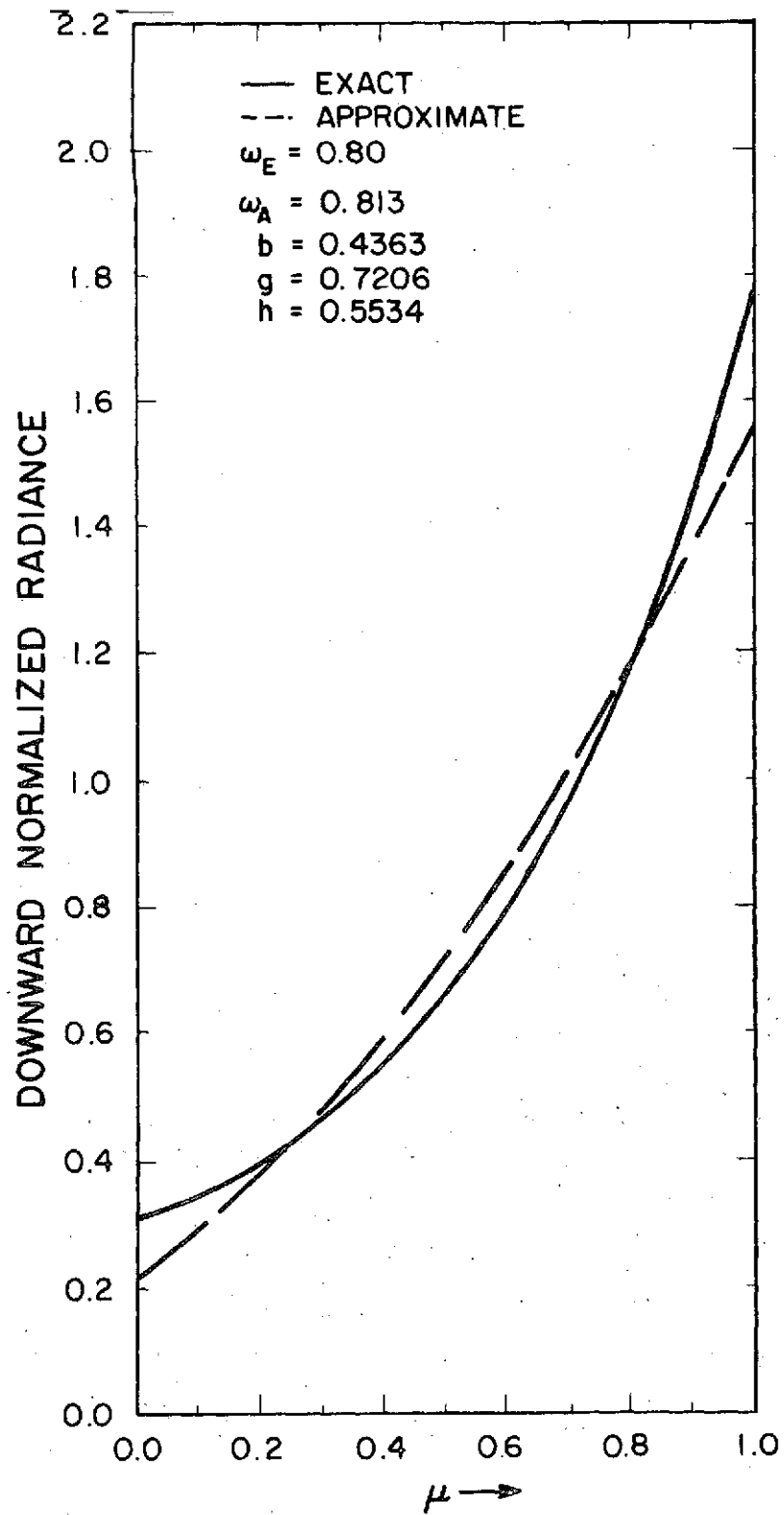
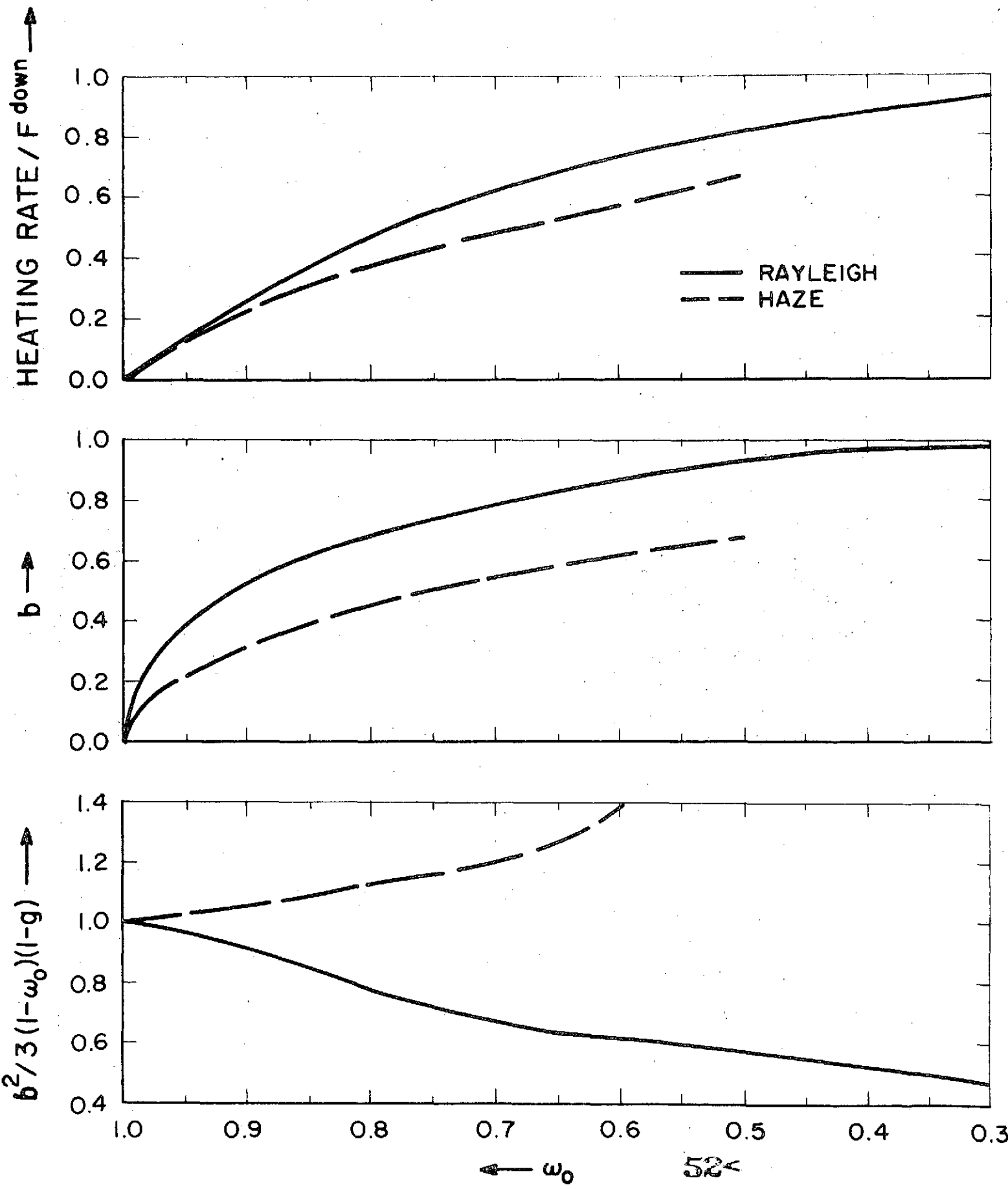
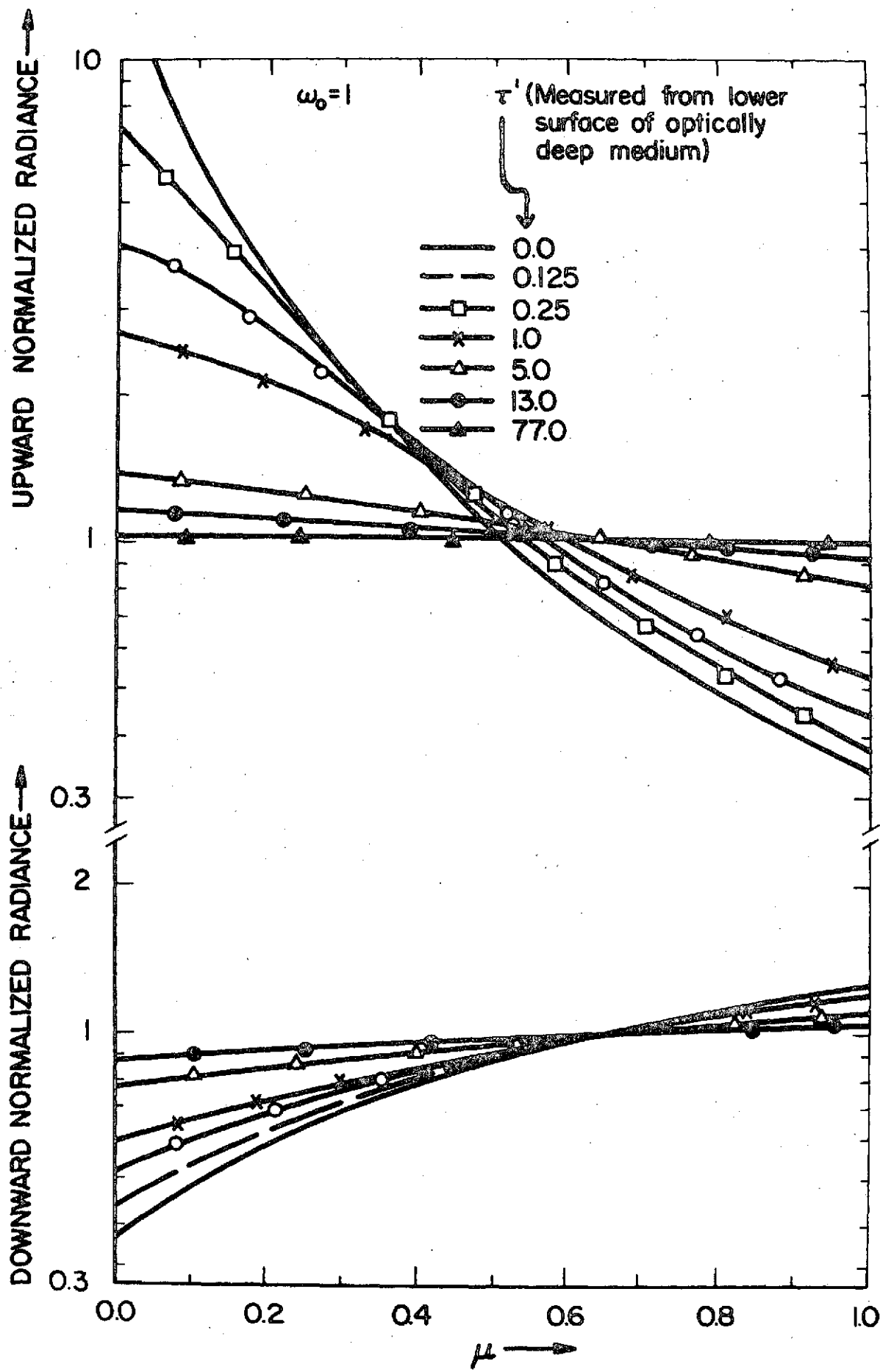


Fig. 18





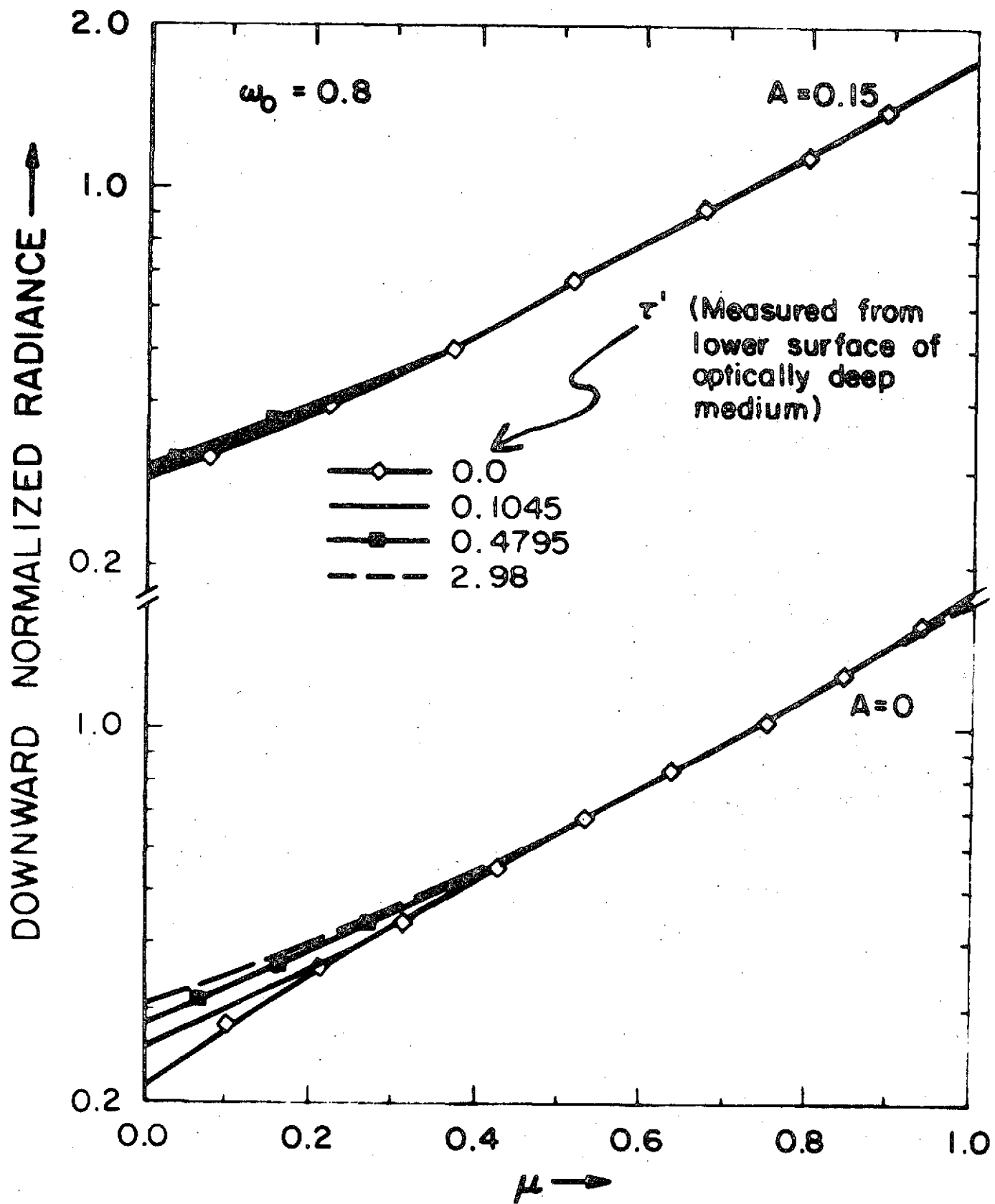
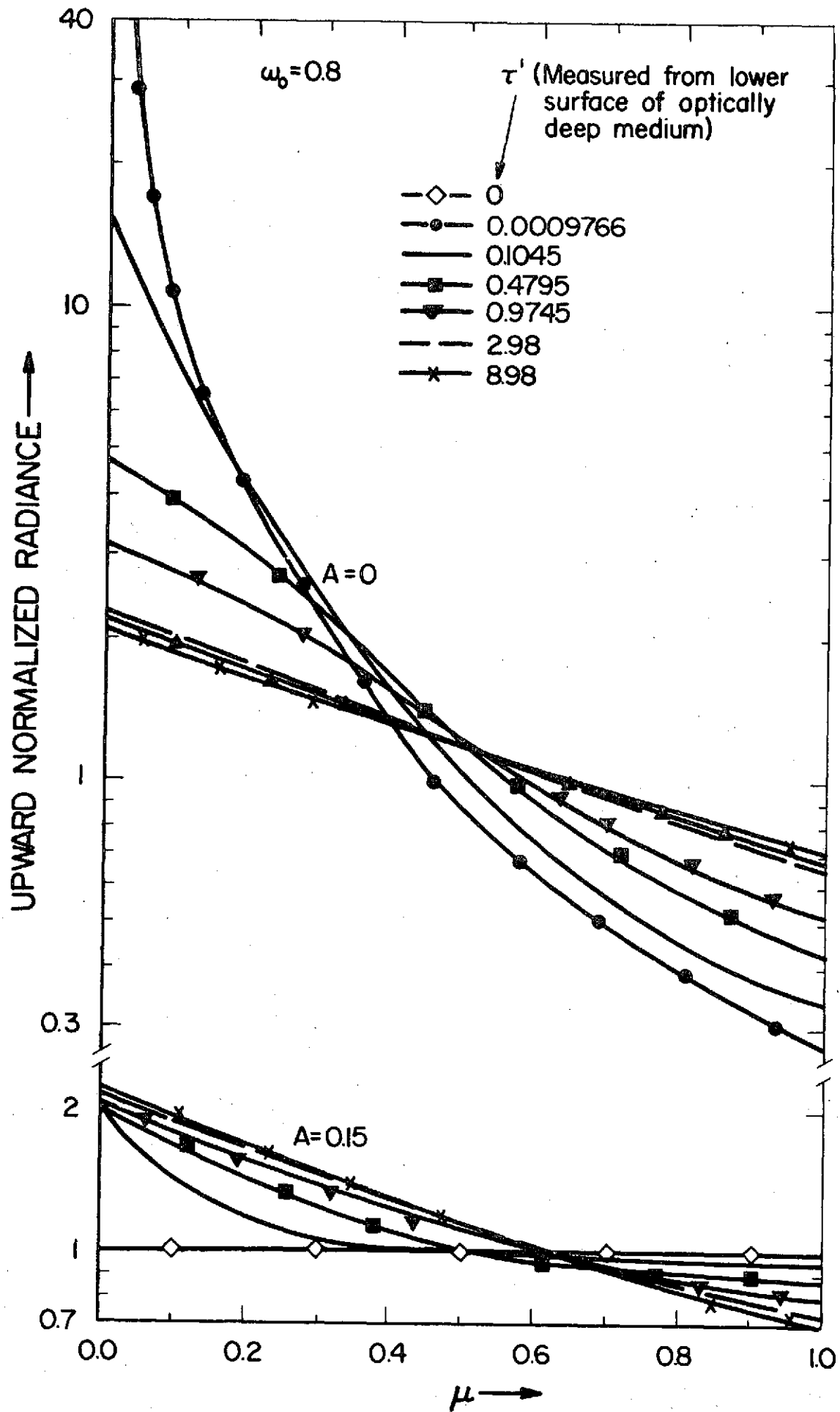


Fig. 21



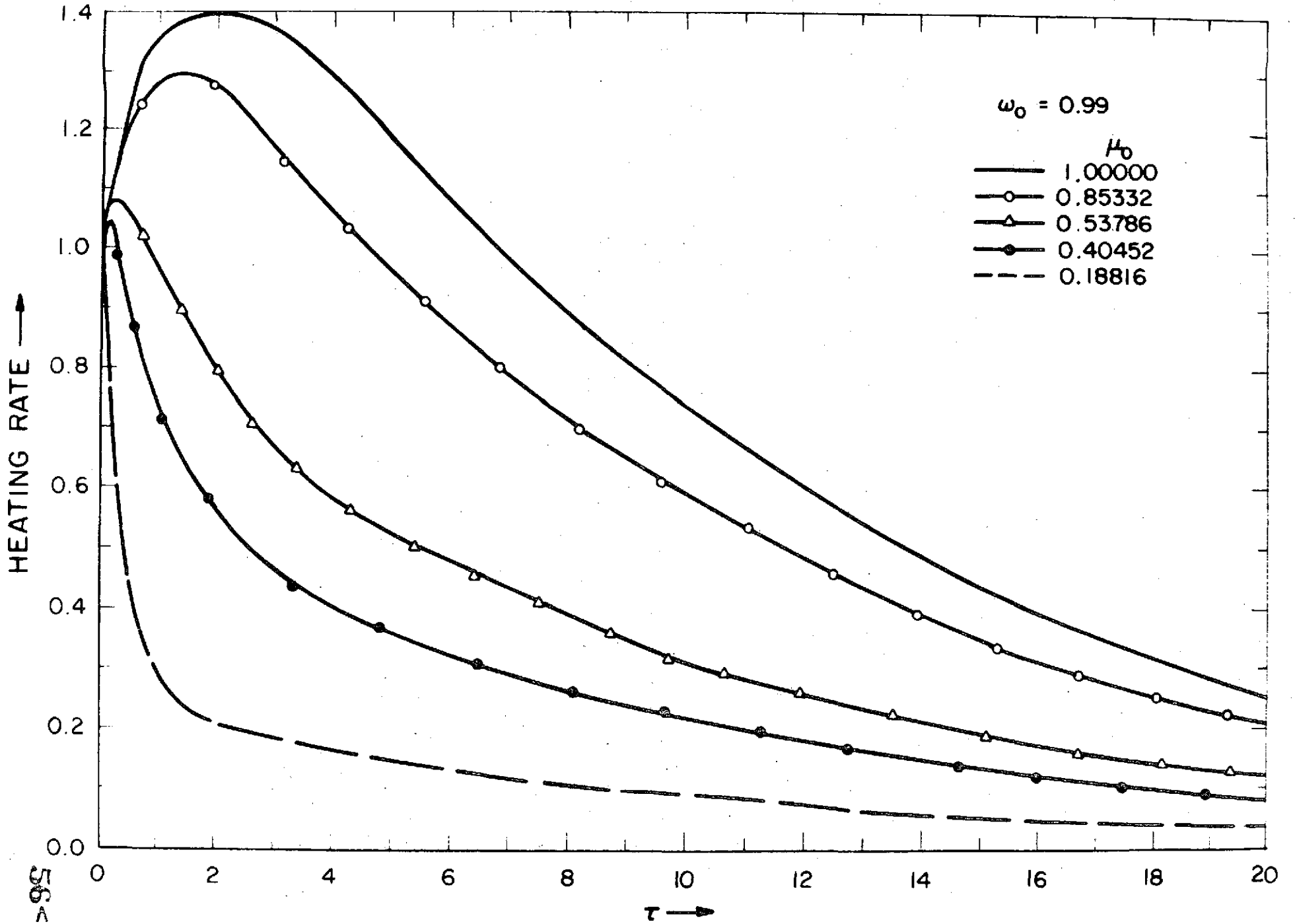


Fig. 23

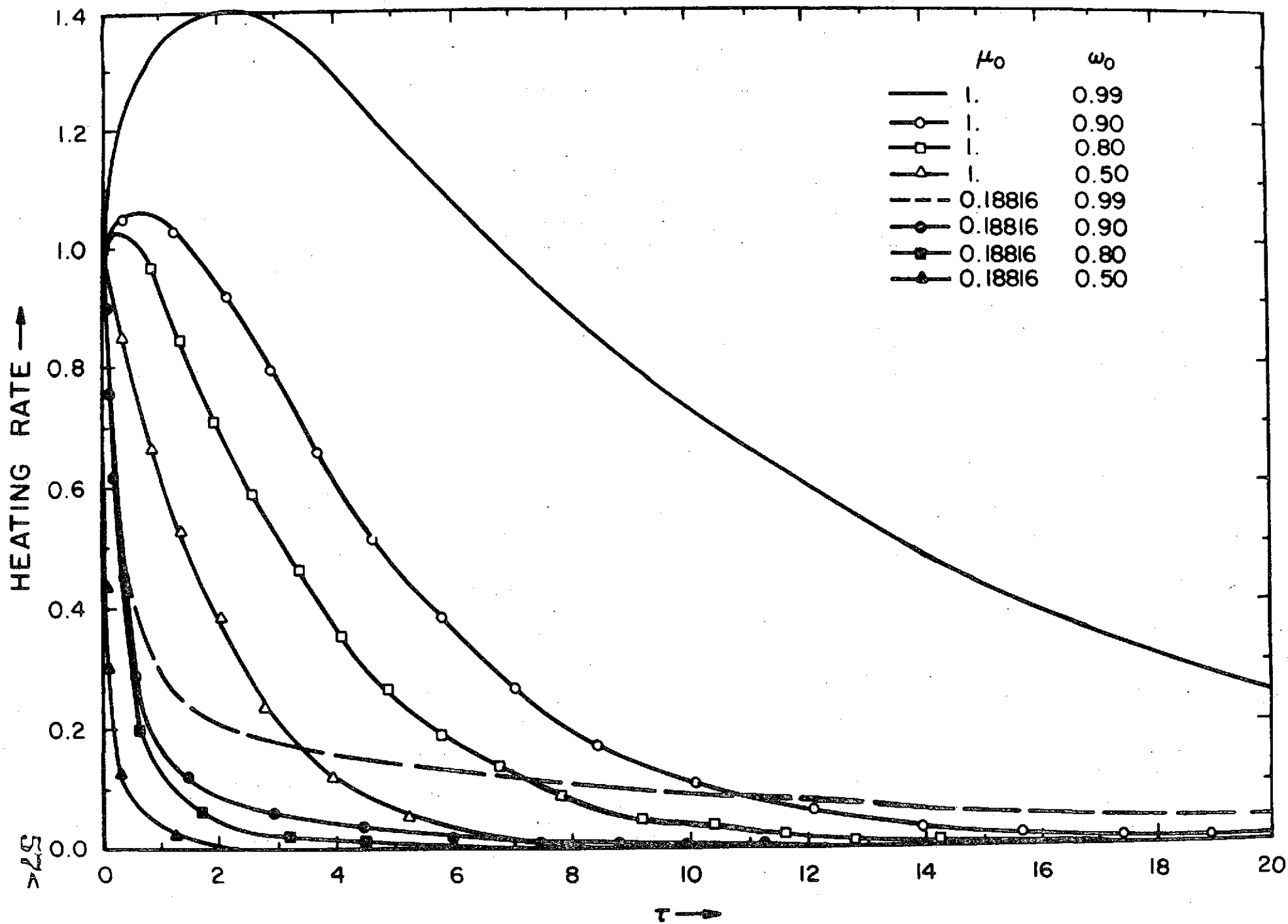


Fig. 24